NNM Backbone Curve Estimation with Near-Resonant Steady State Inputs

Michael Kwarta and Matthew S. Allen

Contents

Abstract

This report presents a detailed description of a new algorithm which allows on a significant speed-ups in Force Appropriation testing. The algorithm is based on the Single Nonlinear Resonant Mode (SNRM) method. It estimates the Nonlinear Normal Mode of the oscillating structure using measurements collected near the nonlinear resonance. The method is first evaluated numerically using a reduced models of flat/curved clamped-clamped beams which exhibit hardening and both softening/hardening responses, respectively. Then the method is employed experimentally to estimate the first NNM of 3D printed flat/curved beams. The results are compared to those obtained using traditional tuning approach.

Keywords: Nonlinear Normal Modes, Force Appropriation Method, Single Nonlinear Resonant Mode Method, Nonlinear Modal Analysis, Nonlinear Frequency Response Functions

1 Introduction

Force appropriation method has long been used for estimating the modal parameters of oscillating structures. The method provides accurate results, but it is unfortunately quite slow and so the structure may be subjected to significant damage over the course of a test. Specifically, the identification of nonlinear systems (conservative [1, 2] and non-conservative [3]) suffers from this drawback, since the nonlinearity usually makes its presence felt when the system vibrates at high-enough amplitudes.

A concept of the Nonlinear Normal Modes is briefly introduced at the beginning of this section. Then the theory and application behind the Force Appropriation method is presented. The most important problems which can be encountered during the Force Appropriation testing are enumerated in section 1.3. On of the goals of this work is to propose an algorithm which helps to overcome issues related to these drawbacks.

1.1 Nonlinear Normal Modes

Response of the vibrating linear mechanical systems can be expressed as a combination of their linear modes. This is possible due to their mutual orthogonality, which can be used to diagonalize the mass and stiffness matrices. Additionally, this property implies natural frequencies being independent of vibration level. In other words, picks of frequency response functions corresponding to different vibration levels will lay one above/below another, forming a straight vertical line on a vibration level vs. frequency plot (see Fig. 1a).

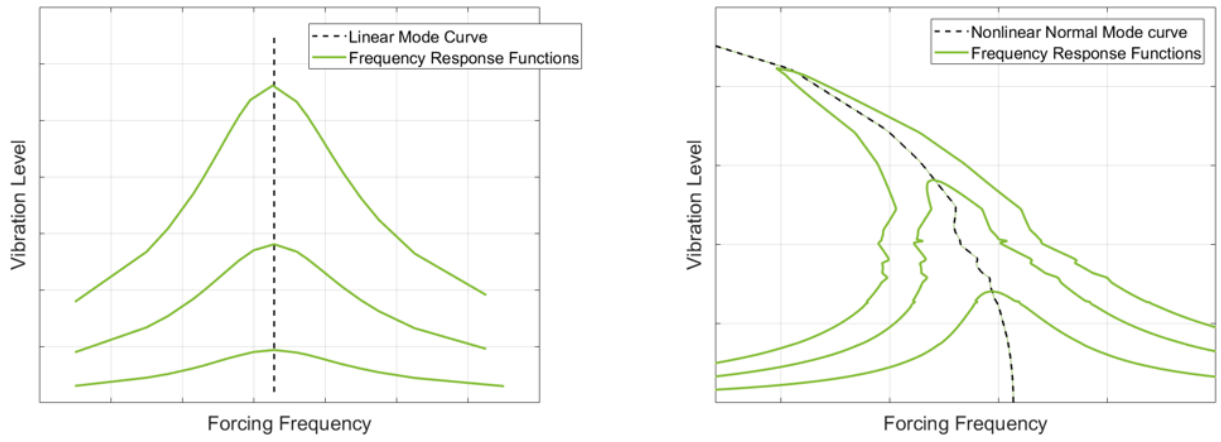

(a) **(b)**

Fig. 1: An example of frequency response functions of **(a)** linear and **(b)** nonlinear systems obtained for different vibration levels.

The principal of superposition does not strictly apply to nonlinear systems. Their natural frequencies are vibration-level-dependent, as shown in e.g. Fig. 1b. Such nonlinear systems have to be examined with methods different than modal decomposition. One of such methods is Force Appropriation described briefly in section 1.2.

1.2 Force Appropriation Method

Force Appropriation is one of the experimental/numerical methods which can be used in e.g. examining if the structure vibrates (or not) at its resonance. It uses two parameters to control the oscillating structure, namely amplitude and frequency of the applied force. Thus, if the forcing amplitude is kept constant - then the forcing frequency can be adjusted in order to bring the vibrating structure to its nonlinear resonance. In other words, if the forcing amplitude is fixed we could tweak the frequency and march up the nonlinear frequency response curve – as shown in Fig. 2: starting from point C, through B, ending up at point A.

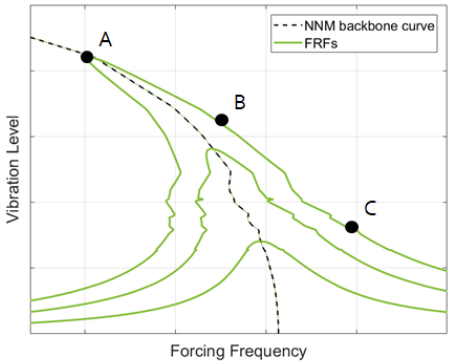

Fig. 2: Force Appropriation Method allows testing the vibrating structure by controlling frequency and amplitude of applied force. Chart shows three frequency response functions obtained for three different forcing amplitudes.

Nonlinear normal modes are periodic motions of the underlying conservative system [1, 4, 5]. Thus the excitation force and velocity are synchronized at the nonlinear resonance and equation of motion can be decoupled *(only if the structure oscillates at its resonance)* into two shown in (1).

$$\mathbf{M}\ddot{\mathbf{x}} + \mathbf{C}\dot{\mathbf{x}} + \mathbf{K}\mathbf{x} + \mathbf{f}_{\mathrm{nl}}(\mathbf{x}) = \mathbf{f}(t) \implies \begin{cases} \mathbf{M}\ddot{\mathbf{x}} + \mathbf{K}\mathbf{x} + \mathbf{f}_{\mathrm{nl}}(\mathbf{x}) = \mathbf{0} \\ \mathbf{C}\dot{\mathbf{x}} = \mathbf{f}(t) \end{cases} \tag{1}$$

This property of mechanical systems is used in Force Appropriation Method to determine how far the vibrating system is from its resonance. Namely, if structure is at resonance – a straight line would be seen on the force vs. velocity signals chart. For the case when the system is not at its resonance – the plot would be an ellipse. The larger the ellipse is the further the structure is from the resonance, as presented in Fig. 3.

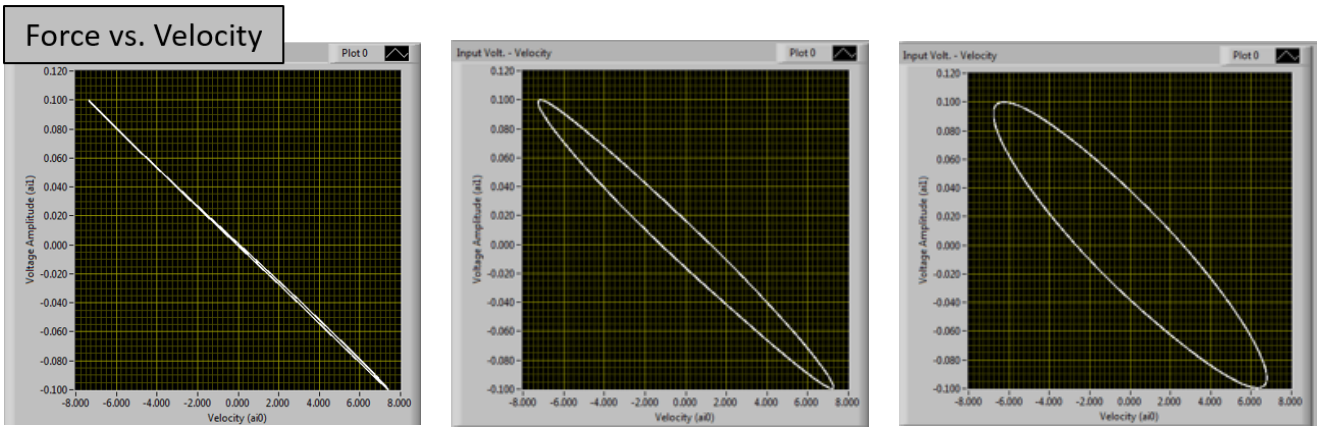

Fig. 3: Force Aprropriation Method compares force and velocity signals to indicate whether the system oscillates at its resonance. Subplots **(a)**, **(b)** and **(c)** correspond to points **A**, **B** and **C** shown in Fig. 3.

Force Appropriation software, which can be used in experimental [6,7] and numerical vibration testing is provided by the members of Structural Dynamics Research Group. Figure 4 shows a print screen of the experimental version of the software, while its numerical counterpart was presented in Fig. 5.

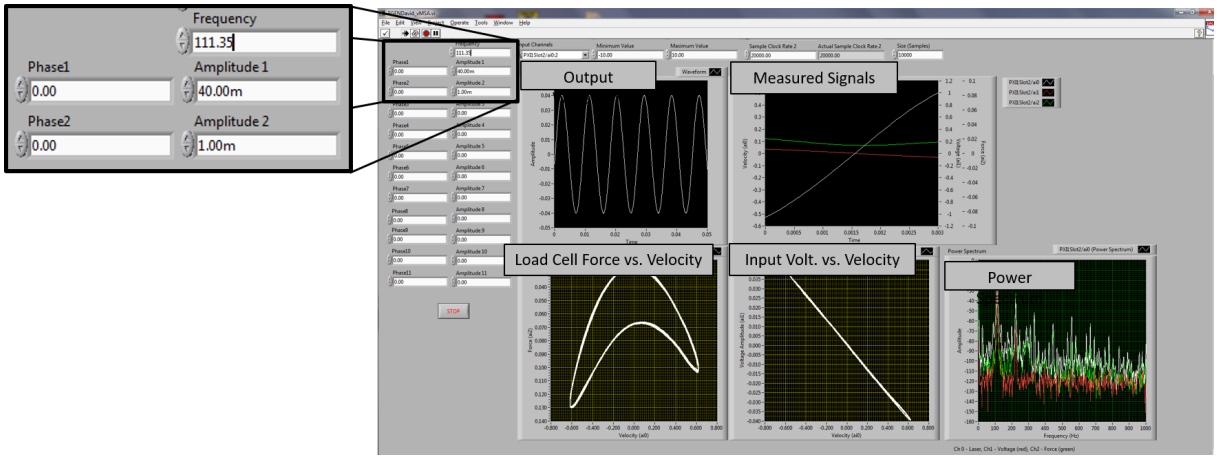

Fig. 4: Screen shot of Harmonic Force Generator Software created using LabView [6,7]. It allows to control forcing frequency and voltage amplitudes of harmonics the structure is excited with.

Numerical version of Force Appropriation computes and prints out value of Mode Indicator Function - feature currently not provided by the experimental software. Moreover, numerical FA allows to take steps back in time (and return to the state of mechanical system from the past).

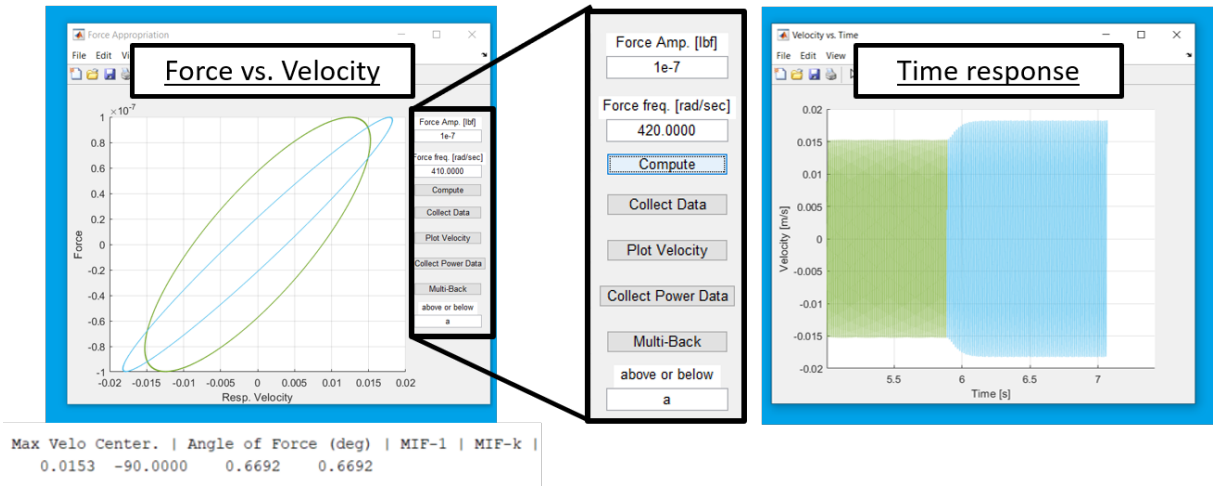

Fig. 5: Screen shot of numerical Force Appropriation software. Besides controlling amplitude and frequency of the force, it allows to e.g. take steps back in time and return to the state of the mechanical system from the past.

It is also worth mentioning that the shape of the curve on force vs. velocity plot does not have to be elliptical. Response may e.g. consist of higher harmonics (Fig. 6a) or be random (response of the system right after falling of the FRF curve, Fig. 6b).

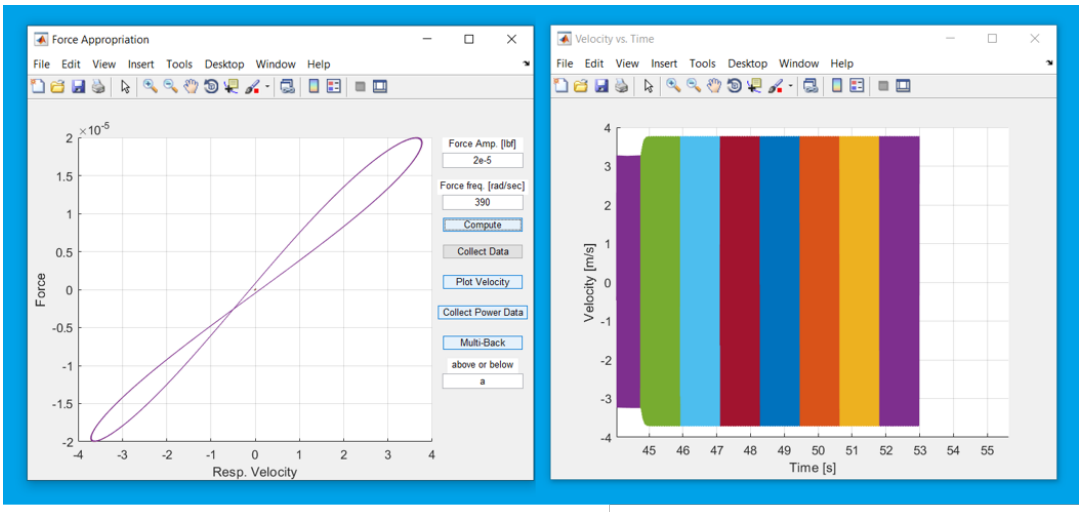


```
Max Velo Center. | Angle of Force (deg) | MIF-1 | MIF-k |
   3.7769  -90.0000    0.9990    0.9991
```

(a)

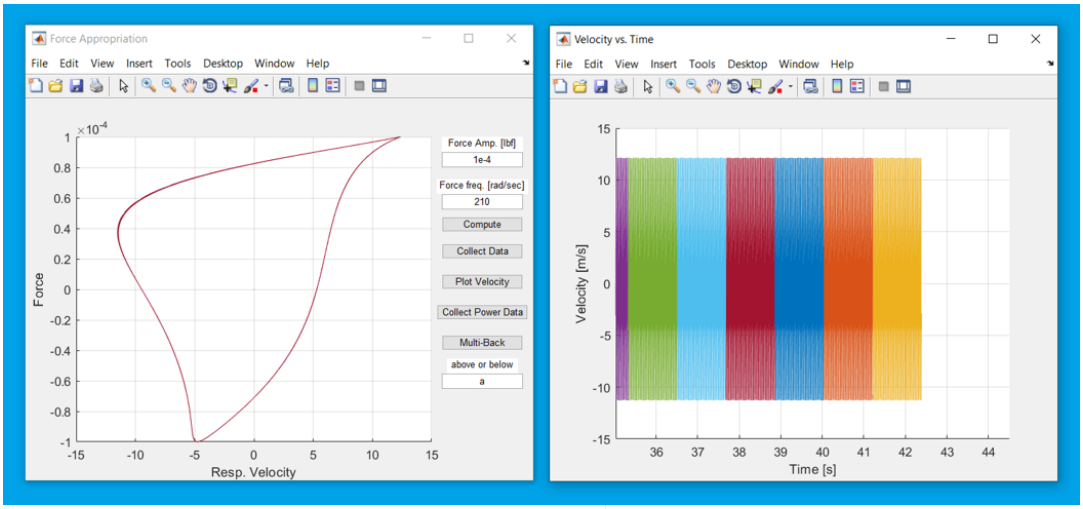


```
Max Velo Center. | Angle of Force (deg) | MIF-1 | MIF-k |
  12.1493  -90.0000    0.3688    0.4191
```

(b)

Fig. 6: Examples of steady state responses which: **(a)** contain higher harmonics; **(b)** is random (response of the system right after falling of the FRF curve).

1.3 Motivation

Force Appropriation is a very simple but powerful and effective method to test the nonlinear oscillating structures. Despite its advantages it still has a few drawbacks. Most important disadvantages of the Force Appropriation method are:

1. Time consuming measurements
2. Premature jump phenomenon
3. Feedback of the oscillating structure

Force appropriation measurements are time consuming because the method allows measurements only for a single forcing amplitude and frequency at a time. If the information about the structure has to be collected for the wider range of frequencies, multiple measurements have to be taken. Additionally, every time the forcing amplitude or frequency is changed, structure needs time to obtain its steady state. Mention about work of ???, who published on how to automatize FA measurements.

When it comes to the second drawback of FA testing – collecting data of the resonating nonlinear structure is sometimes not possible. Structure can switch from lag to lead branch of the FRF, before reaching the actual turning point. This experimental testing issue is called the *premature jump phenomenon* and can lead to incorrect estimation of the nonlinear FRFs picks.

Feedback of the vibrating structure usually leads to distortions of the excitation force and can impact the quality of the measured test data. Naturally, the closer the structure is to its resonance the larger the feedback is what lowers the quality of the measurements. The algorithm we proposed in this work addresses all three drawbacks of Force Appropriation testing enumerated above and allows to overcome the issues caused by them.

2 Algorithm Overview

2.1 Theoretical Background

The algorithm proposed in this report is an extension of the linear vibrations theory, where the response of the system can be expressed as a combination of its modes, see Eq. (2).

$$V = \sum_{k=1}^{N_{lin}} \frac{\mathbf{\Phi}_k \mathbf{\Phi}_k^T \mathbf{F} \Omega}{\omega_{0,k}^2 - \Omega^2 + 2i\zeta_k \omega_{0,k} \Omega} \Bigg|_{\substack{\text{pt. of max.} \\ \text{deflection}}} \tag{2}$$

Since the goal of this work is system identification of the nonlinear systems – model presented in Eq. (2) had to be modified in order to be able to analyze such systems. The concept of Single Nonlinear Resonant Mode (SNRM), which was first proposed in [8], brings Eq. (2) to a form that allows for nonlinear SI, see Eq (3). The method requires vibration modes to be well-separated and assumes no internal resonances between them.

The SNRM method extracts one of the modes from the sum in Eq. (2) and models it as nonlinear, while keeping the rest of the modes linear and superimposing them, see Eq. (3). The strengths of the method are: *(i)* its simple mathematical form and *(ii)* a straight–forward correlation to the linear vibration theory. Visualization of quantities V_j^{nl} and V^{lin} is presented in Fig. 7.

$$V^{\text{meas}} \approx V^{model} = \underbrace{\left.\frac{\tilde{\mathbf{\Phi}}_j \tilde{\mathbf{\Phi}}_j^T \mathbf{F}\Omega}{\tilde{\omega}_{0,j}^2 - \Omega^2 + 2i\tilde{\zeta}_j\tilde{\omega}_{0,j}\Omega}\right|_{\substack{\text{pt. of max.}\\ \text{deflection}}}}_{V_j^{nl}} + \underbrace{\sum_{\substack{k=1\\k\neq j}}^{N_{lin}} \left.\frac{\mathbf{\Phi}_k \mathbf{\Phi}_k^T \mathbf{F}\Omega}{\omega_{0,k}^2 - \Omega^2 + 2i\zeta_k\omega_{0,k}\Omega}\right|_{\substack{\text{pt. of max.}\\ \text{deflection}}}}_{V^{lin}} \tag{3}$$

In Eq. (3): Ω is the forcing frequency; $\mathbf{\Phi}_i$, $\omega_{0,i}$, ζ_i are the mode shape, natural frequency and modal damping ratio of the i-th mode, respectively; $\mathbf{F}$ is the distribution of a sinusoidal force excitation; j is index of the dominant mode, and N_{lin} denotes the number of relevant linear modes. The quantities marked ($\sim$) vary with the vibration level.

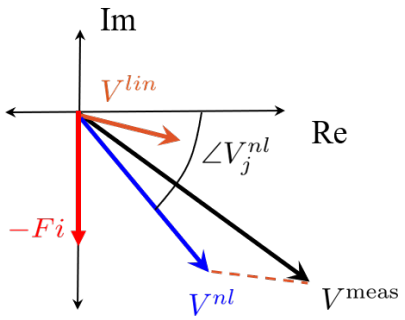

Fig. 7: Visualization of quantities V_j^{nl} and V^{lin} from Eq. (3)

As presented in the Eq. (3), the nonlinearity is modeled by representing three physical parameters, namely $\omega_{0,i}$, ζ_i, $\mathbf{\Phi}_i$ as functions of the vibration level. In this work, the vibration level is represented usually with velocity amplitude (unless specified otherwise).

The proposed algorithm uses models for magnitude and phase of the velocity complex amplitude, see Eqs. (4) and (5).

$$\left\|V^{\text{meas}}\right\| = \left\|V_j^{nl} + V^{lin}\right\| \tag{4}$$

$$\angle\left(V_j^{nl}\right) = \angle\left(V^{\text{meas}} - V^{lin}\right) = \tan^{-1}\left(\frac{-2\tilde{\zeta}_j\tilde{\omega}_{0,j}\Omega}{\tilde{\omega}_{0,j}^2 - \Omega^2}\right) \tag{5}$$

For clarity let us also define:

$$v = \left\|V^{\text{meas}}\right\| \tag{$\star$}$$

$$\tilde{\varphi}_j^{\text{vel}} = \angle\left(V_j^{nl}\right) \tag{$\star\star$}$$

Equation (5), which is a model for the phase of velocity complex amplitude, can be used in expressing nonlinear natural frequency as a function of nonlinear damping. Namely, Eq. (5) can be brought to a form of quadratic function (6). The real solution of Equation (6) always exists, as indicated in Eq. (7). Thus, it can be used to express $\tilde{\omega}_{0,j}$ as a function of $\tilde{\zeta}_j$, see Eq. (8) and/or Eq. (9).

$$\tilde{\omega}_{0,j}^2 + \frac{-2\tilde{\zeta}_j\Omega}{\tan(\tilde{\varphi}_j^{\text{vel}})}\,\tilde{\omega}_{0,j} - \Omega^2 = 0 \tag{6}$$

$$\Delta = 2\Omega\ (\tilde{\zeta}_j^2 + \tan^2(\tilde{\varphi}_j^{\mathrm{vel}})) > 0 \tag{7}$$

$$\tilde{\omega}_{0,j} = f(\tilde{\zeta}_j) = \frac{-\tilde{\zeta}_j \pm \sqrt{\tilde{\zeta}_j^2 + \tan^2(\tilde{\varphi}_j^{\mathrm{vel}})}}{\tan(\tilde{\varphi}_j^{\mathrm{vel}})}\ \Omega \tag{8}$$

$$\tilde{\omega}_{0,j} = f(\tilde{\zeta}_j) = \begin{cases} \dfrac{-\tilde{\zeta}_j + \sqrt{\tilde{\zeta}_j^2 + \tan^2(\tilde{\varphi}_j^{\mathrm{vel}})}}{\tan(\tilde{\varphi}_j^{\mathrm{vel}})}\ \Omega & \text{if} \quad \tan(\tilde{\varphi}_j^{\mathrm{vel}}) > 0 \\ \text{(meas. point above the NNM; phase lag)} \\ \dfrac{-\tilde{\zeta}_j - \sqrt{\tilde{\zeta}_j^2 + \tan^2(\tilde{\varphi}_j^{\mathrm{vel}})}}{\tan(\tilde{\varphi}_j^{\mathrm{vel}})}\ \Omega & \text{if} \quad \tan(\tilde{\varphi}_j^{\mathrm{vel}}) < 0 \\ \text{(meas. point below the NNM; phase lead)} \end{cases} \tag{9}$$

2.2 Algorithm Stages

The objective of the algorithm is to estimate the NNM curve using, as an input, quantities $(v,\ \Omega,\ \tilde{\varphi}_j^{\mathrm{vel}})$ measured in the vicinity of the nonlinear resonance. The algorithm proposed here consists of three stages:

1. Collect data in the laboratory or simulated test and compute $(v,\ \Omega,\ \tilde{\varphi}_j^{\mathrm{vel}})$.
2. Use Eqs. (4) and (9) to assign $\tilde{\zeta}_j$ and $\tilde{\omega}_{0,j}$ values to every $(v,\ \Omega,\ \tilde{\varphi}_j^{\mathrm{vel}})$ point.
3. Express $\tilde{\omega}_{0,j}$ and $\tilde{\zeta}_j$ as (e.g. piecewise linear) functions of the velocity magnitude v.

The result of the above three-stages-long procedure is obtaining $\tilde{\omega}_{0,j} = \omega_{0,j}(v)$ and $\tilde{\zeta}_j = \zeta_j(v)$. Former quantity is searched NNM backbone, while the latter function shows how the nonlinear damping ratio changes with vibration level if the structure is modeled using Eq. (3).

The results are validated against the data collected in the physical/numerical tests. Namely, the estimated NNM points $(v_*,\ \omega_*,\ -90°)$ obtained for a certain forcing level are compared with the NNM points measured during the tests using the same excitation level. Additionally, Eq. (3) allows for modeling the FRF curve, as presented e.g. in [9], with the $(v_*,\ \omega_*,\ -90°)$ as a start point. Hence, the accuracy of the method can also be evaluated via comparison between the FRF curves modeled and measured experimentally or numerically.

According to a well-known saying: *a picture is worth a thousand words*. Thus, it would probably be more convenient and clearer to present each of the algorithm's steps on a few plots. The algorithm stages as well as the validation steps are visualized in Tables from 1 to 7.

Tab. 1: Overview of the Algorithm: Algorithm's objective.

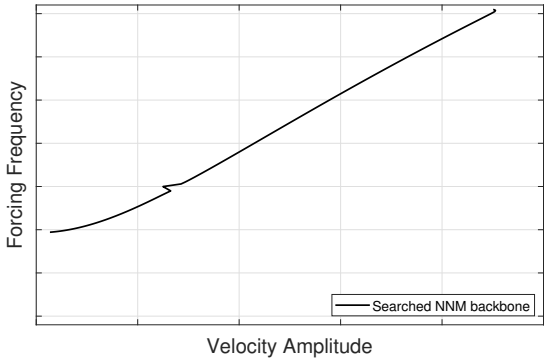

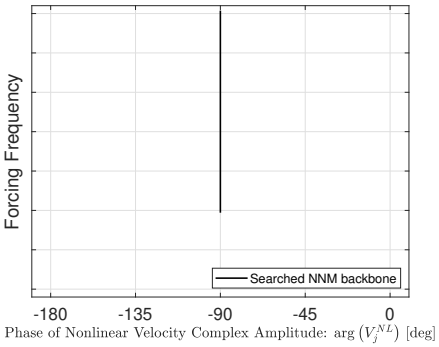

Algorithm's objective: Estimate the NNM curve.

Tab. 2: Overview of the Algorithm: Step 1.

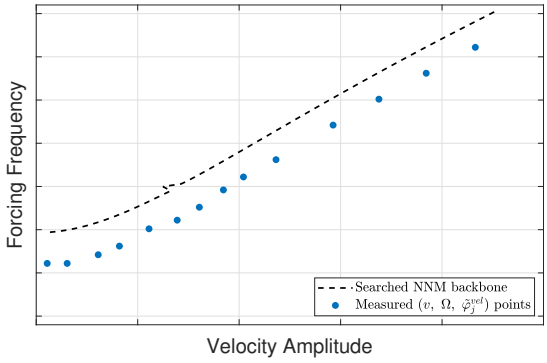

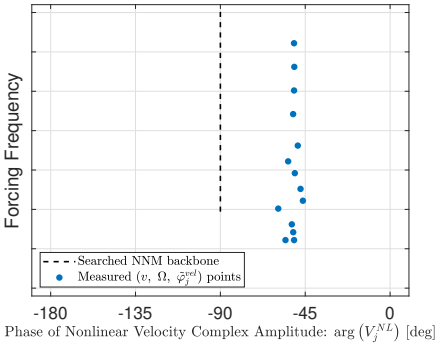

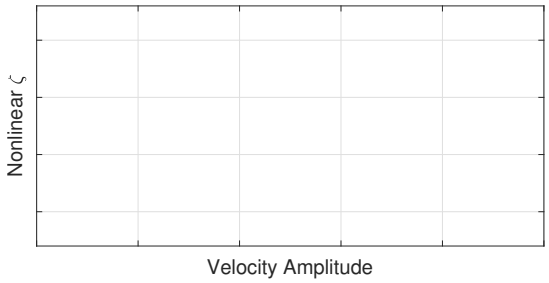

Algorithm's objective: Estimate the NNM curve.

Step 1: Collect near-resonant test points $(v,\ \Omega,\ \tilde{\varphi}_j^{\mathrm{vel}})$.

Tab. 3: Overview of the Algorithm: Step 2.

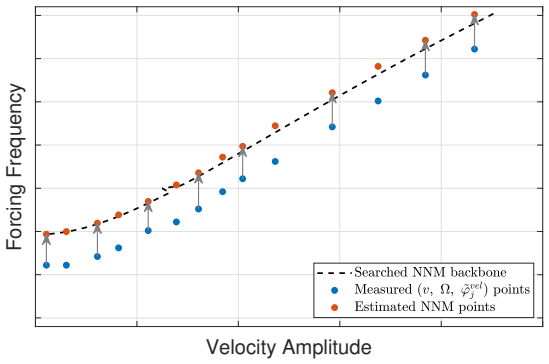

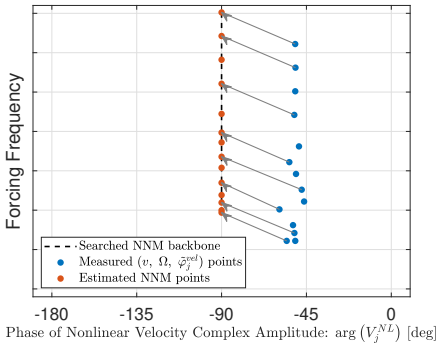

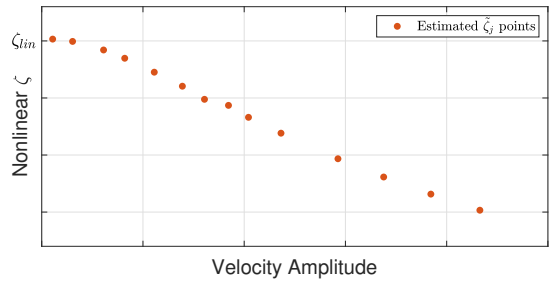

Algorithm's objective: Estimate the NNM curve.

Step 1: Collect near-resonant test points $(v,\ \Omega,\ \tilde{\varphi}_j^{\text{vel}})$.

Step 2: Assign $\tilde{\zeta}_j$ and $\tilde{\omega}_{0,j}$ to each $(v,\ \Omega,\ \tilde{\varphi}_j^{\text{vel}})$ point via solving Eq. (4) and Eq. (9).

Tab. 4: Overview of the Algorithm: Step 3.

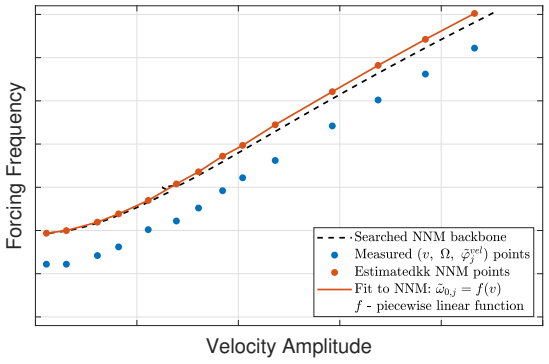

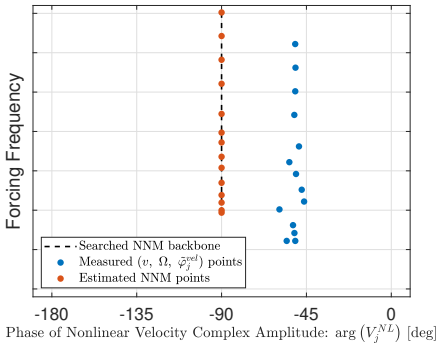

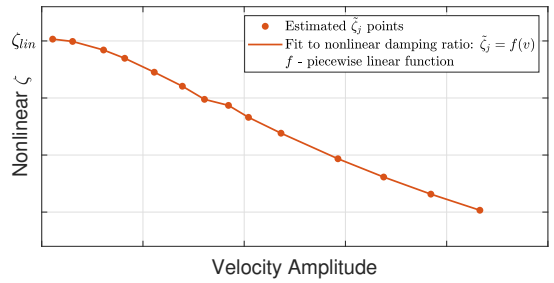

Algorithm's objective: Estimate the NNM curve.

Step 1: Collect near-resonant test points $(v,\ \Omega,\ \tilde{\varphi}_j^{\text{vel}})$.

Step 2: Assign $\tilde{\zeta}_j$ and $\tilde{\omega}_{0,j}$ to each $(v,\ \Omega,\ \tilde{\varphi}_j^{\text{vel}})$ point via solving Eq. (4) and Eq. (9).

Step 3: Express $\tilde{\zeta}_j$ and $\tilde{\omega}_{0,j}$ as functions of v.

Tab. 5: Overview of the Algorithm: Method Validation – Step 1.

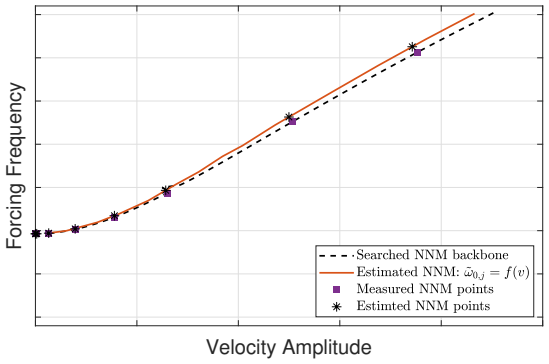

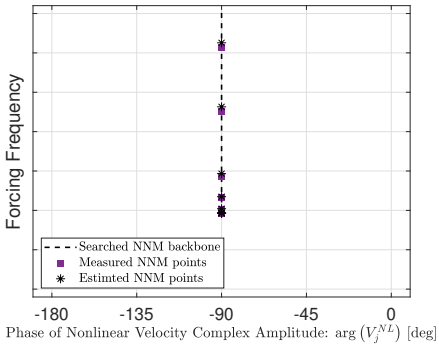

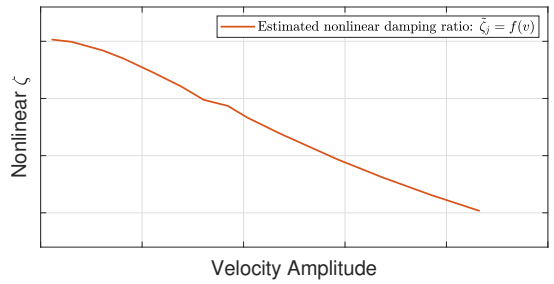

Method Validation

Step 1: Compare measued NNM points with points $(v_*,\ \omega_*)$ at which the FRF and NNM curves intersect for a certain forcing level.

At the nonlinear resonance, forcing frequency and nonlinear modal frequency are equal: $\Omega = \tilde{\omega}_{0,j}(v_*) = \omega_*$. Hence, Eq. (4) at this point can be simplified:

$$v_* = \left\| \left(\frac{\mathbf{\Phi}_j \mathbf{\Phi}_j^T \mathbf{F}}{2i\tilde{\zeta}_j \omega_*} + \mathbf{V}^{lin}(\omega_*) \right) \Big|_{\substack{\text{pt. of max.} \\ \text{deflection}}} \right\|$$

Tab. 6: Overview of the Algorithm: Method Validation – Step 2.

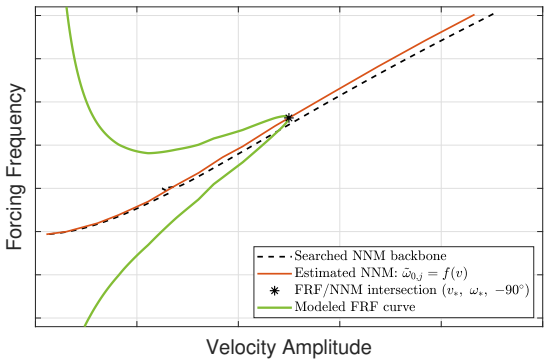

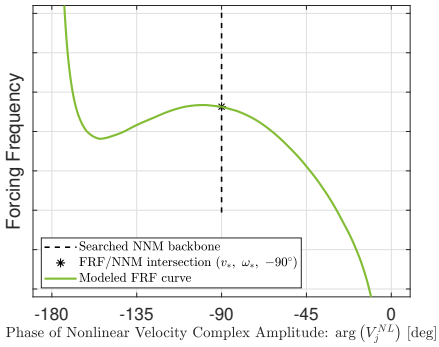

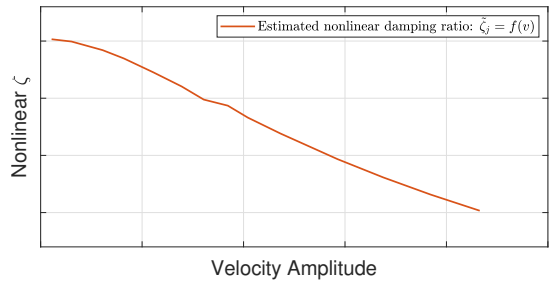

Method Validation

Step 1: Compare measued NNM points with points $(v_*,\ \omega_*)$ at which the FRF and NNM curves intersect for a certain forcing level.

Step 2: Model the upper (lag) and lower (lead) branches of the FRF using Eq. (4) with $(v_*,\ \omega_*)$ as a start point.

Tab. 7: Overview of the Algorithm: Method Validation – Step 3.

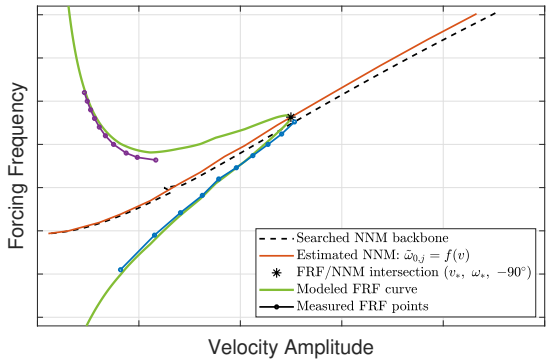

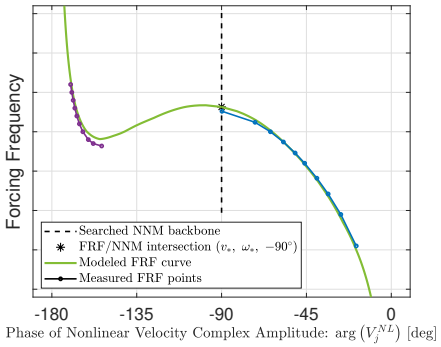

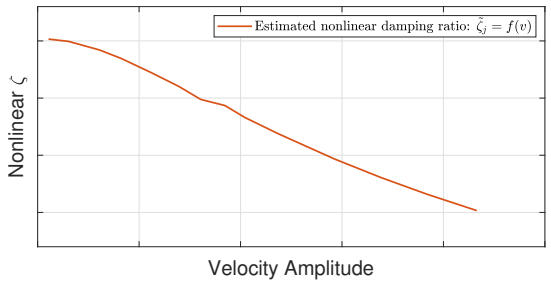

Method Validation

Step 1: Compare measued NNM points with points (v_*, ω_*) at which the FRF and NNM curves intersect for a certain forcing level.

Step 2: Model the upper (lag) and lower (lead) branches of the FRF using Eq. (4) with (v_*, ω_*) as a start point.

Step 3: Validate modeled FRF against the one obtained from the experimental or numerical measurements.

3 Case Study

In this section the results from four case studies are presented. The algorithm is used to estimate the Nonlinear Normal Mode backbone curve of flat and curved beams. The method is tested with data generated numerically using a reduced models experiencing no or slight modal interaction. Then the method is used to estimate the NNM backbones of 3D printed beams made of polylactide (PLA). Results are presented and validated in a similar way to the one proposed in section 2.2.

3.1 Flat Clamped-Clamped Beam – Numerical Example

The numerical Force Appropriation test is performed on a *flat beam* with clamped-clamped boundary conditions. The beam is identical to the one studied on [10] and it has dimensions and mechanical properties presented in Tab. 8.

Tab. 8: Dimensions and mechanical properties of the numerical flat clamped-clamped beam.

Lenght [mm]	Width [mm]	Thickness [mm]
228.6	12.7	0.787
Young's modulus [GPa]	**Density $[\frac{\text{kg}}{\text{m}^3}]$**	**Shear modulus [GPa]**
204.8	7870	80.0

The beam is modeled with 40 beam elements resulting in a total of 246 DOFs and it is excited with an uniformly distributed sinusoidal force (Fig. 8). The test is performed on the 4-mode ROM including modes 1, 3, 5 and 7. Mode 1 is simulated as a nonlinear one and the response of the three remaining modes is superimposed linearly.

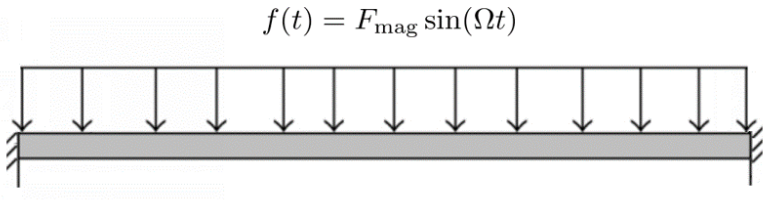

Fig. 8: Uniformly distributed sinusoidal force is used to excite the numerical flat beam.

Table 9 shows the results obtained after running three-stages-long algorithm described in section 2.2. Plots corresponding to each of the validation steps are presented in Tables from 10 to 12. Results are briefly commented at the end of this section.

Tab. 9: Flat CC-Beam Numerical Example. Results.

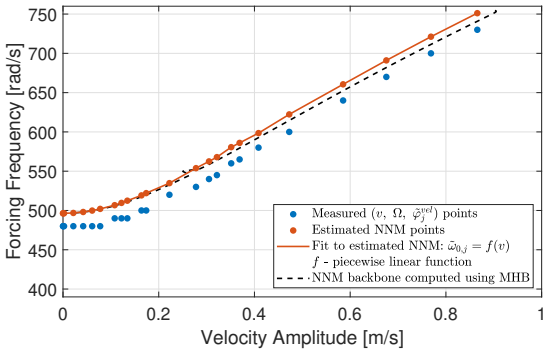

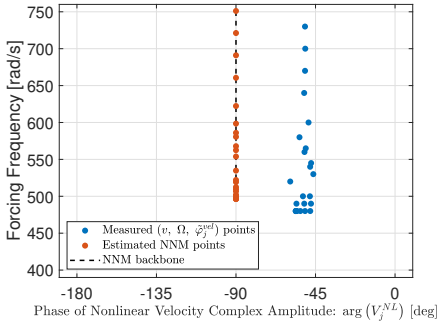

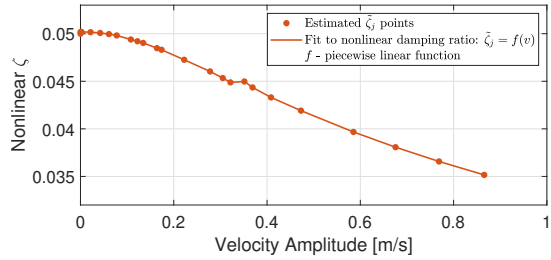

1) Near resonant data points have been collected; MIF $\in$ (0.5, 0.7).

2) The NNM points are estimated using Eqs. (4) and (9).

3) Piecewise linear function is used to approximate the NNM curve.

4) The NNM backbone computed with the presented algorithm is compared to the solution obtained using the Multi-Harmonic Balance Method (cite one or two papers).

Tab. 10: Flat CC-Beam Numerical Example. Validation – Step 1.

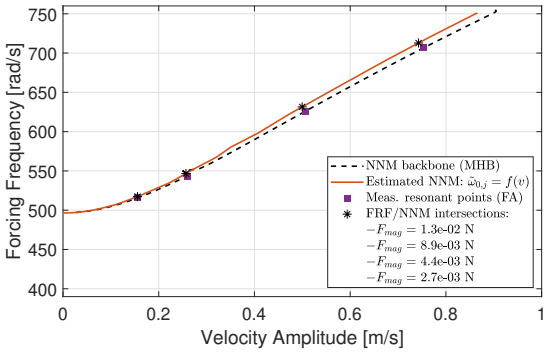

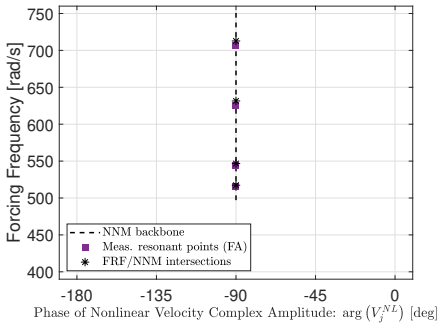

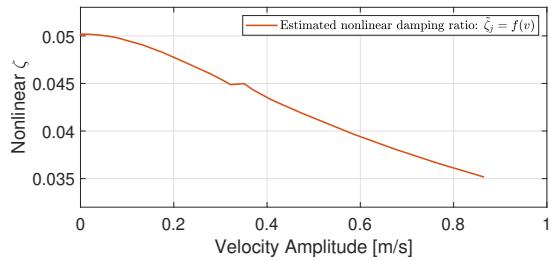

Validation

Points (v_*, ω_*) at which the FRF and NNM curves intersect for a certain forcing level are compared to the NNM points measured numerically.

At the nonlinear resonance, forcing frequency and nonlinear modal frequency are equal: $\Omega = \tilde{\omega}_{0,j}(v_*) = \omega_*$. Hence, Eq. (4) at this point can be simplified:

$$v_* = \left\| \left(\frac{\mathbf{\Phi}_j \mathbf{\Phi}_j^T \mathbf{F}}{2i\tilde{\zeta}_j \omega_*} + \mathbf{V}^{lin}(\omega_*) \right) \Big|_{\substack{\text{pt. of max.} \\ \text{deflection}}} \right\|$$

Tab. 11: Flat CC-Beam Numerical Example. Validation – Step 2.

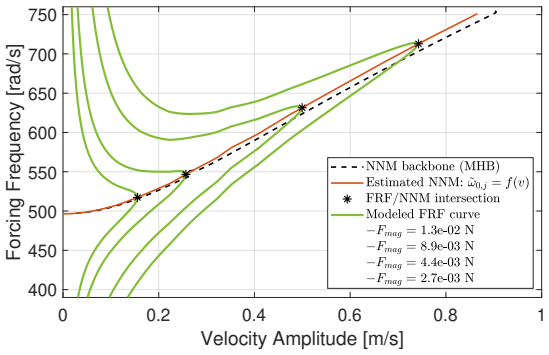

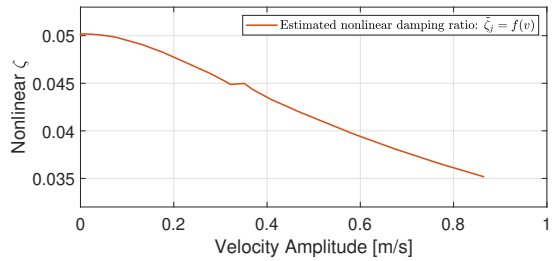

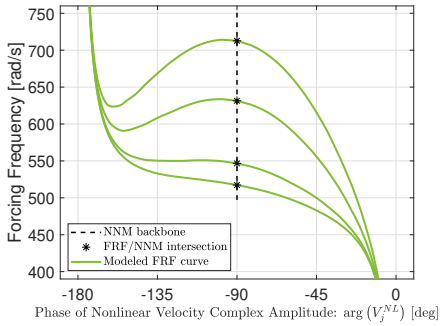

Validation

The upper (lag) and lower (lead) branches of the FRF are modeled using Eq. (4) with $(v_*,\ \omega_*)$ as a start point.

Tab. 12: Flat CC-Beam Numerical Example. Validation – Step 3.

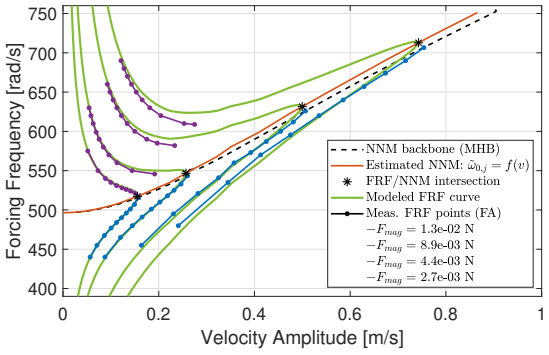

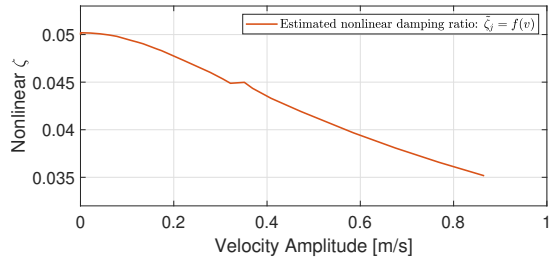

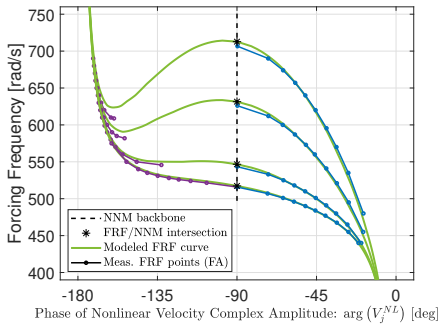

Validation

The upper (lag) and lower (lead) branches of the FRF are modeled using Eq. (4) with $(v_*,\ \omega_*)$ as a start point.

Modeled FRF is validated against the one measured using the numerical Force Appropriation method.

Comments

1. Proposed algorithm estimates the NNM backbone with a satisfactory precision using near-resonant test data (MIF $\in (0.5,\ 0.7)$).

2. NNM points estimated using Eq. (4) for a given forcing magnitude are close enough to the resonant points measured numerically using Force Appropriation method and the same force amplitude.

3. Nonlinear frequency response functions measured numerically and computed using Eq. (4) match each other to a satisfactory extent.

4. The algorithm allows on a significant reduction in the time spent on numerical measurements. Finding NNM curve using FA software takes approximately 2 hours. With the proposed algorithm, it takes approximately 20 minutes.

5. Besides estimating the NNM backbone curve, the algorithm expresses nonlinear damping ratio as a function of velocity amplitude. In this particular example $\tilde{\zeta}_j$ is found as a decreasing function of the vibration level.

3.2 Curved Clamped-Clamped Beam – Numerical Example

The numerical Force Appropriation test is performed on a *curved beam* with clamped-clamped boundary conditions. The beam has dimensions and mechanical properties presented in Tab. 13.

Tab. 13: Dimensions and mechanical properties of the numerical curved clamped-clamped beam.

Lenght [mm]	Width [mm]	Thickness [mm]	Radius of curvature [m]
304.8	12.7	0.508	11.43

Young's modulus [GPa]	Density $[\frac{\text{kg}}{\text{m}^3}]$	Poisson's Ratio
204	7860	0.29

The beam is modeled with 400 shell elements resulting in a total of 3030 DOFs and is excited with an uniformly distributed sinusoidal force (Fig. 9). The test is performed on the 1-mode ROM (1st mode) which is modeled as nonlinear.

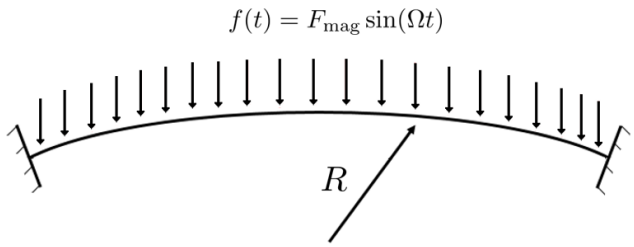

Fig. 9: Uniformly distributed sinusoidal force is used in exciting the numerical curved beam.

Table 14 shows the results obtained after running three-stages-long algorithm described in section 2.2. Plots corresponding to the validation part are presented in Tables from 15 to 29. Results are briefly commented at the end of this section.

Tab. 14: Curved CC-Beam Numerical Example. Results.

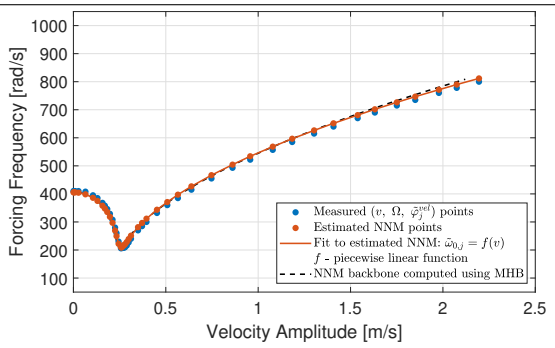

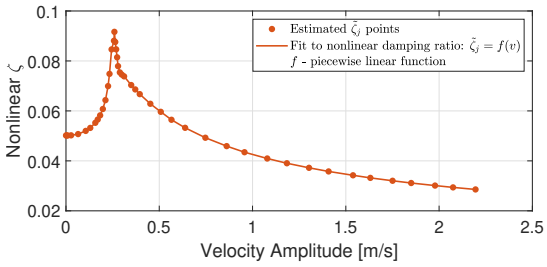

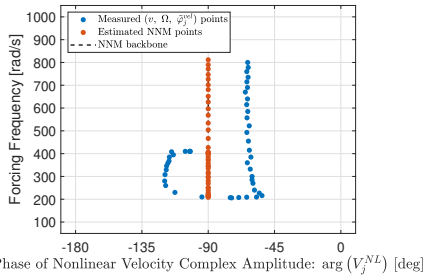

1) Near resonant data points have been collected; MIF $\in (0.7842,\ 1.0)$.

2) The NNM points are estimated using Eqs. (4) and (9).

3) Piecewise linear function is used to approximate the NNM curve.

4) The NNM backbone computed with the presented algorithm is compared to the solution obtained using the Multi-Harmonic Balance Method (cite one or two papers).

Tab. 15: Curved CC-Beam Numerical Example. Comparison of the NNM points modeled and measured numerically using Force Appropriation.

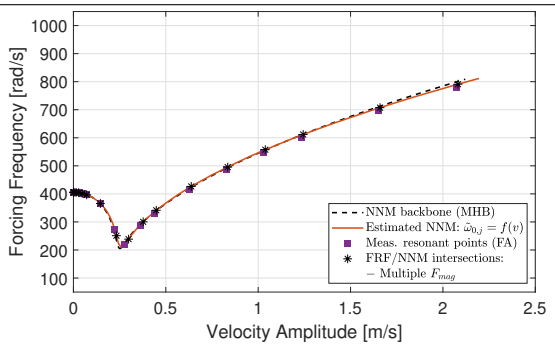

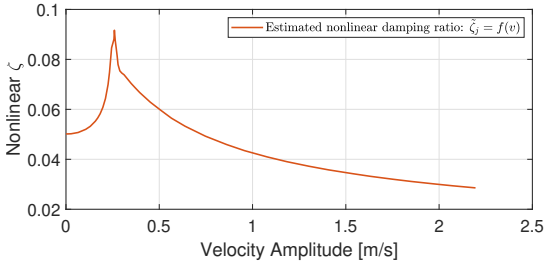

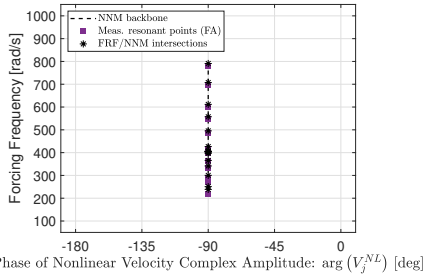

Validation

Points $(v_*,\ \omega_*)$ at which the FRF and NNM curves intersect for a certain forcing level are compared to the NNM points measured numerically.

At the nonlinear resonance, forcing frequency and nonlinear modal frequency are equal: $\Omega = \tilde{\omega}_{0,j}(v_*) = \omega_*$. Hence, Eq. (4) at this point can be simplified:

$$v_* = \left\| \left(\frac{\boldsymbol{\Phi}_j \boldsymbol{\Phi}_j^T \mathbf{F}}{2i\tilde{\zeta}_j \omega_*} + \mathbf{V}^{lin}(\omega_*) \right) \Big|_{\substack{\text{pt. of max.} \\ \text{deflection}}} \right\|$$

Tab. 16: Curved CC-Beam Numerical Example. Comparison of the nonlinear FRF curves modeled and measured numerically using Force Appropriation. FRF ID: 5

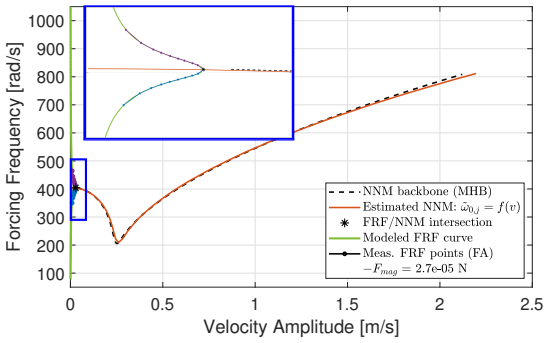

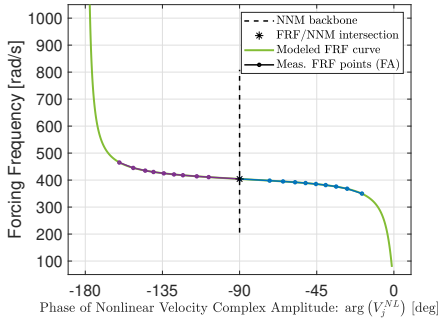

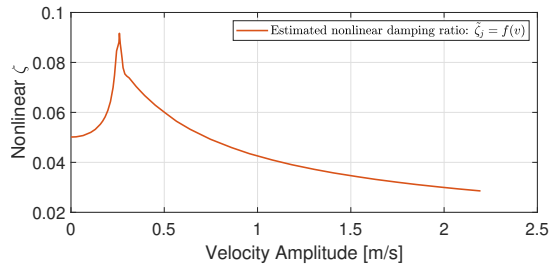

Validation

The upper (lag) and lower (lead) branches of the FRF are modeled using Eq. (4) with $(v_*,\ \omega_*)$ as a start point.

Modeled FRF is validated against the one measured using the numerical Force Appropriation method.

Tab. 17: Curved CC-Beam Numerical Example. Comparison of the nonlinear FRF curves modeled and measured numerically using Force Appropriation. FRF ID: 6

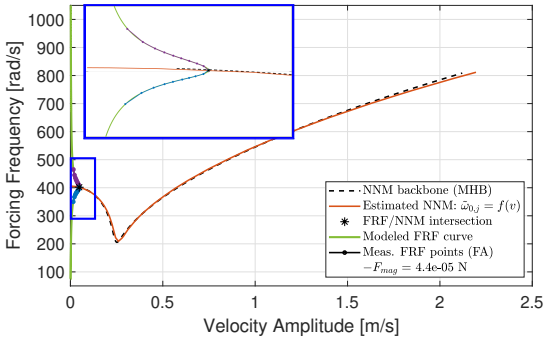

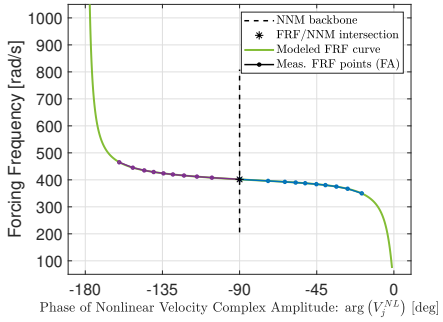

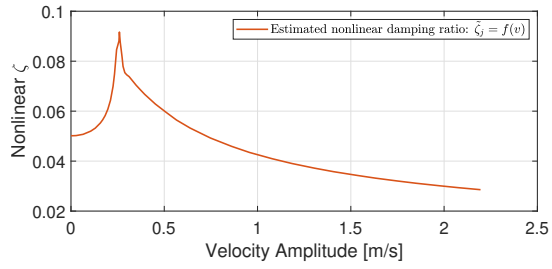

Validation

The upper (lag) and lower (lead) branches of the FRF are modeled using Eq. (4) with $(v_*,\ \omega_*)$ as a start point.

Modeled FRF is validated against the one measured using the numerical Force Appropriation method.

Tab. 18: Curved CC-Beam Numerical Example. Comparison of the nonlinear FRF curves modeled and measured numerically using Force Appropriation. FRF ID: 7

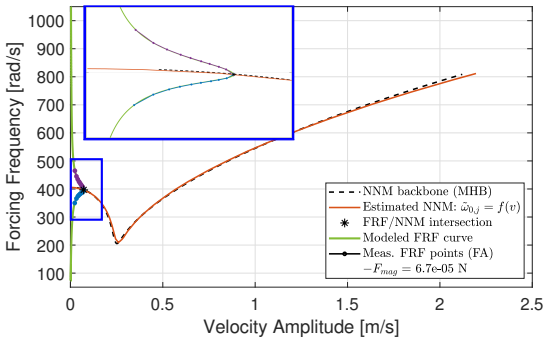

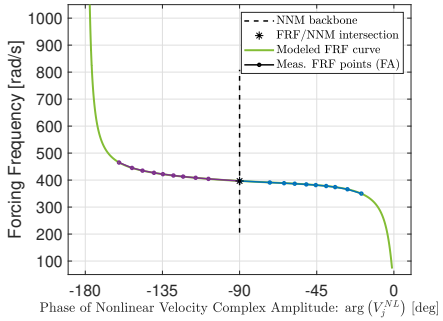

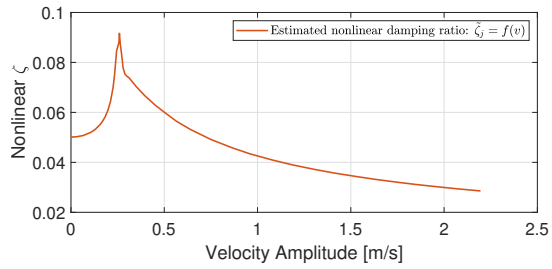

Validation

The upper (lag) and lower (lead) branches of the FRF are modeled using Eq. (4) with $(v_*,\ \omega_*)$ as a start point.

Modeled FRF is validated against the one measured using the numerical Force Appropriation method.

Tab. 19: Curved CC-Beam Numerical Example. Comparison of the nonlinear FRF curves modeled and measured numerically using Force Appropriation. FRF ID: 8

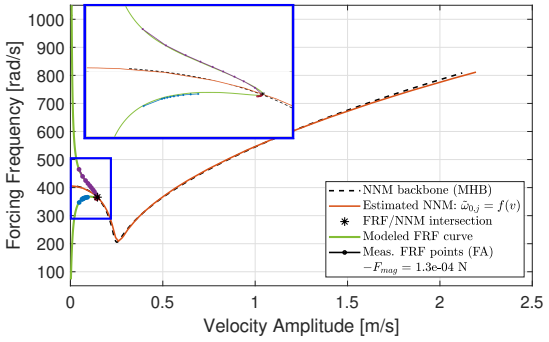

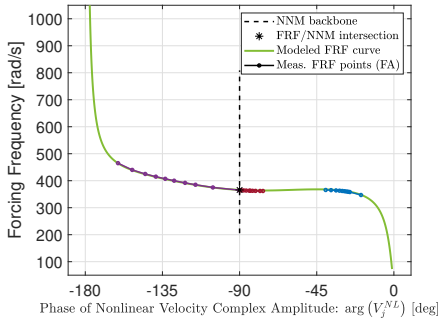

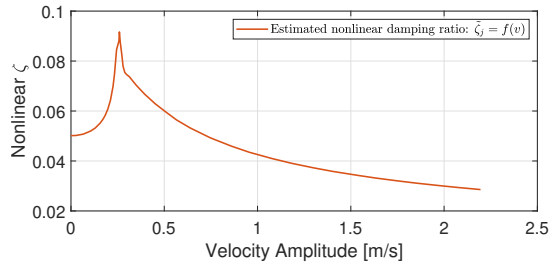

Validation

The upper (lag) and lower (lead) branches of the FRF are modeled using Eq. (4) with $(v_*,\ \omega_*)$ as a start point.

Modeled FRF is validated against the one measured using the numerical Force Appropriation method.

Tab. 20: Curved CC-Beam Numerical Example. Comparison of the nonlinear FRF curves modeled and measured numerically using Force Appropriation. FRF ID: 9

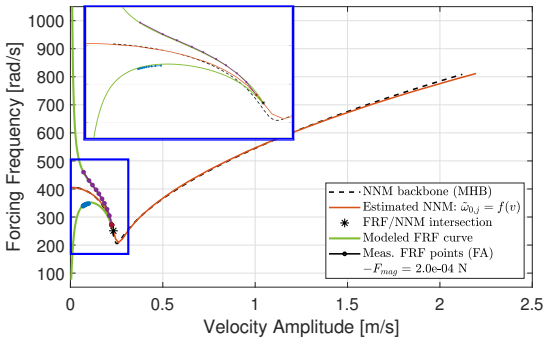

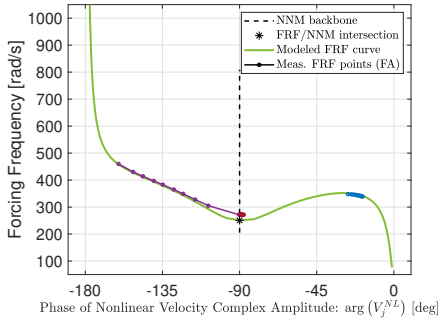

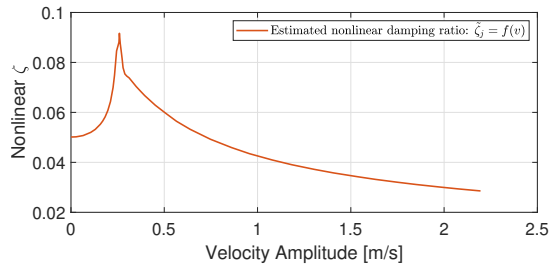

Validation

The upper (lag) and lower (lead) branches of the FRF are modeled using Eq. (4) with $(v_*,\ \omega_*)$ as a start point.

Modeled FRF is validated against the one measured using the numerical Force Appropriation method.

Tab. 21: Curved CC-Beam Numerical Example. Comparison of the nonlinear FRF curves modeled and measured numerically using Force Appropriation. FRF ID: 10

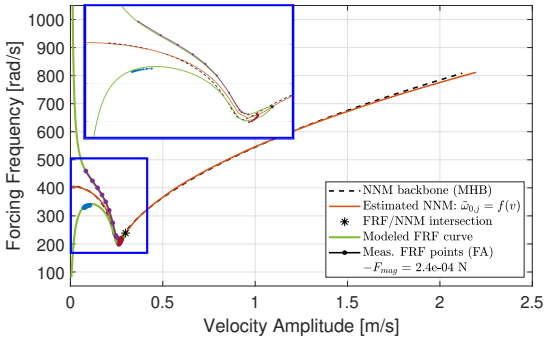

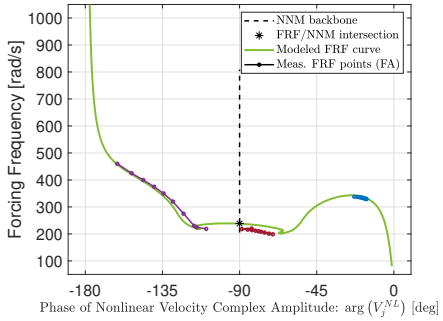

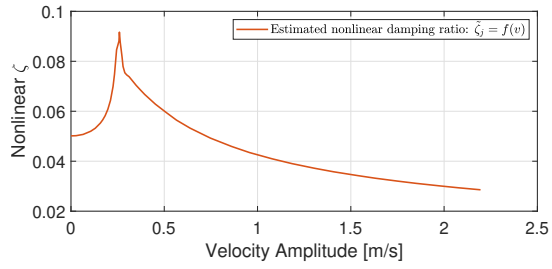

Validation

The upper (lag) and lower (lead) branches of the FRF are modeled using Eq. (4) with $(v_*,\ \omega_*)$ as a start point.

Modeled FRF is validated against the one measured using the numerical Force Appropriation method.

Tab. 22: Curved CC-Beam Numerical Example. Comparison of the nonlinear FRF curves modeled and measured numerically using Force Appropriation. FRF ID: 11

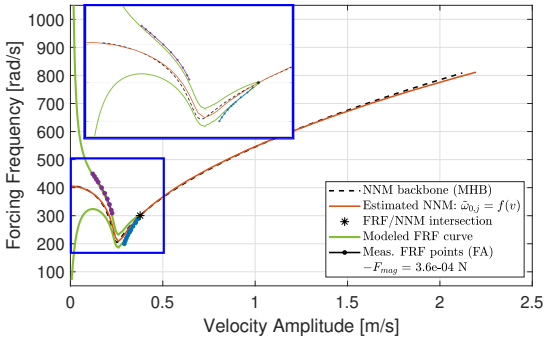

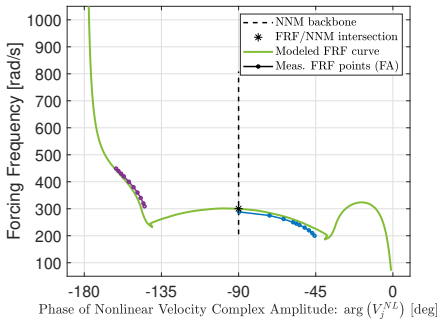

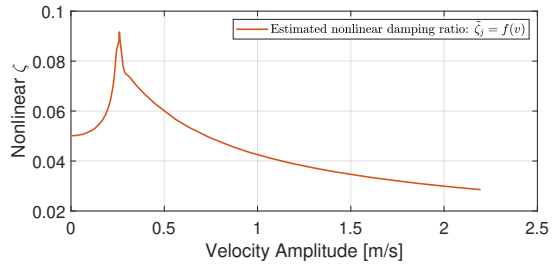

Validation

The upper (lag) and lower (lead) branches of the FRF are modeled using Eq. (4) with $(v_*,\ \omega_*)$ as a start point.

Modeled FRF is validated against the one measured using the numerical Force Appropriation method.

Tab. 23: Curved CC-Beam Numerical Example. Comparison of the nonlinear FRF curves modeled and measured numerically using Force Appropriation. FRF ID: 12

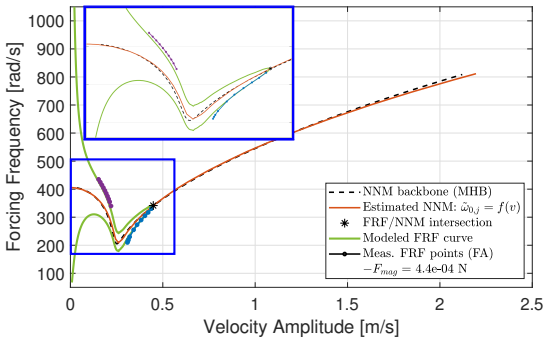

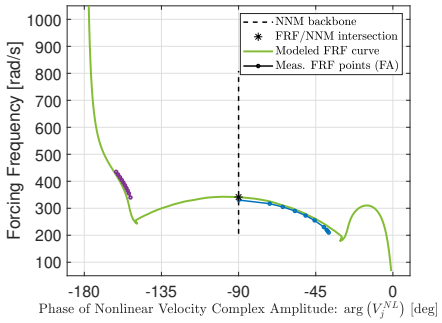

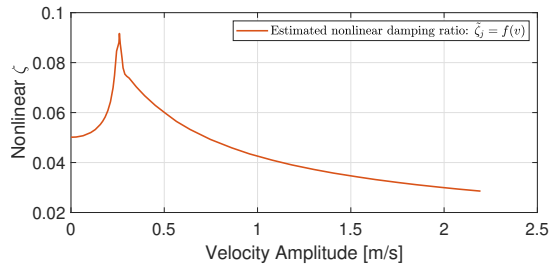

Validation

The upper (lag) and lower (lead) branches of the FRF are modeled using Eq. (4) with $(v_*,\ \omega_*)$ as a start point.

Modeled FRF is validated against the one measured using the numerical Force Appropriation method.

Tab. 24: Curved CC-Beam Numerical Example. Comparison of the nonlinear FRF curves modeled and measured numerically using Force Appropriation. FRF ID: 13

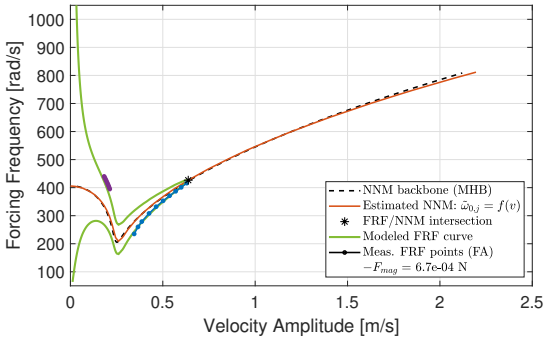

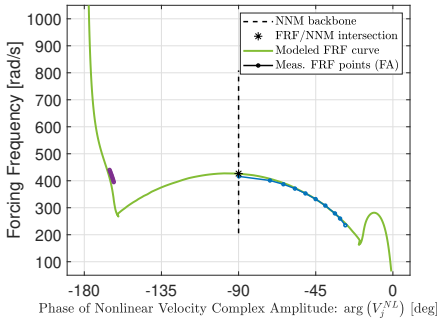

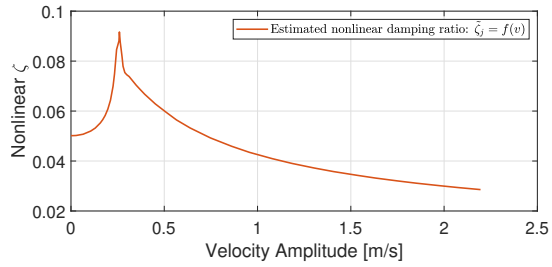

Validation

The upper (lag) and lower (lead) branches of the FRF are modeled using Eq. (4) with $(v_*,\ \omega_*)$ as a start point.

Modeled FRF is validated against the one measured using the numerical Force Appropriation method.

Tab. 25: Curved CC-Beam Numerical Example. Comparison of the nonlinear FRF curves modeled and measured numerically using Force Appropriation. FRF ID: 14

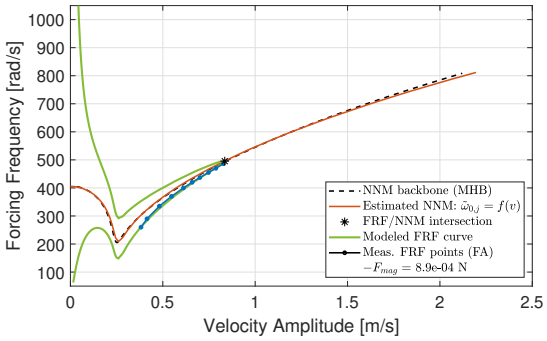

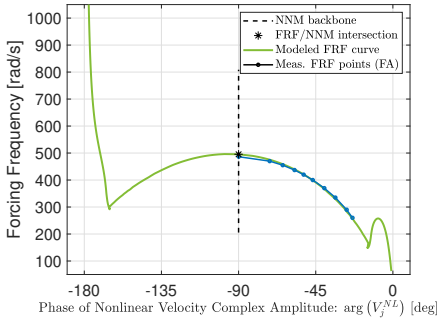

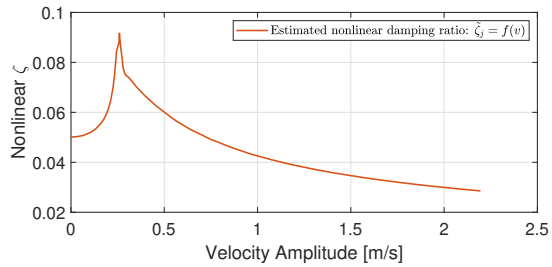

Validation

The upper (lag) and lower (lead) branches of the FRF are modeled using Eq. (4) with $(v_*,\ \omega_*)$ as a start point.

Modeled FRF is validated against the one measured using the numerical Force Appropriation method.

Tab. 26: Curved CC-Beam Numerical Example. Comparison of the nonlinear FRF curves modeled and measured numerically using Force Appropriation. FRF ID: 15

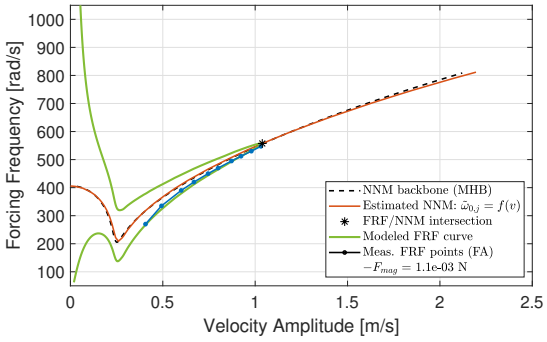

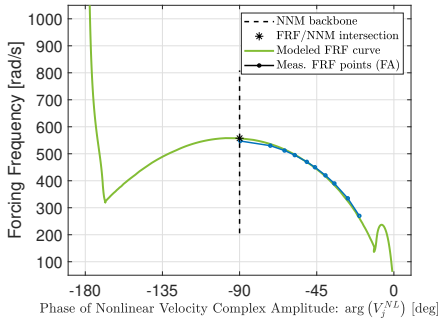

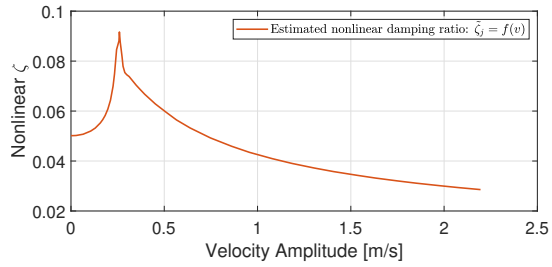

Validation

The upper (lag) and lower (lead) branches of the FRF are modeled using Eq. (4) with $(v_*,\ \omega_*)$ as a start point.

Modeled FRF is validated against the one measured using the numerical Force Appropriation method.

Tab. 27: Curved CC-Beam Numerical Example. Comparison of the nonlinear FRF curves modeled and measured numerically using Force Appropriation. FRF ID: 16

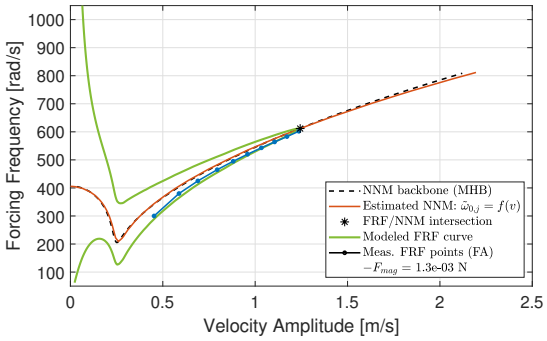

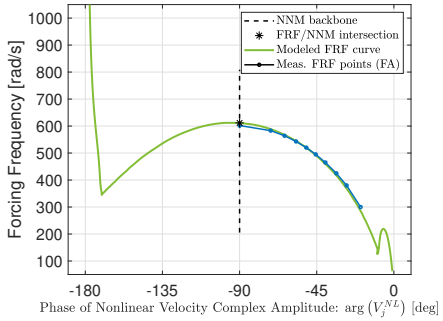

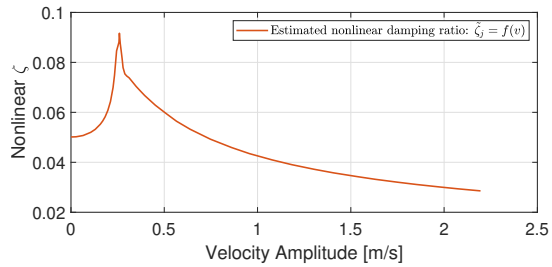

Validation

The upper (lag) and lower (lead) branches of the FRF are modeled using Eq. (4) with $(v_*,\ \omega_*)$ as a start point.

Modeled FRF is validated against the one measured using the numerical Force Appropriation method.

Tab. 28: Curved CC-Beam Numerical Example. Comparison of the nonlinear FRF curves modeled and measured numerically using Force Appropriation. FRF ID: 17

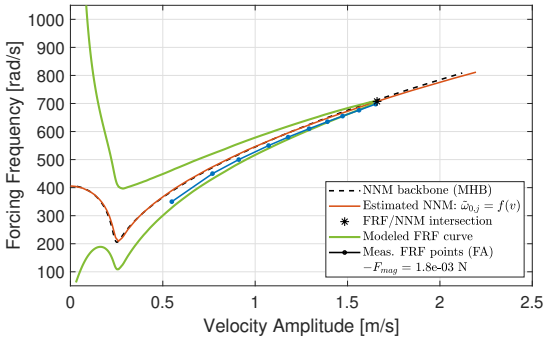

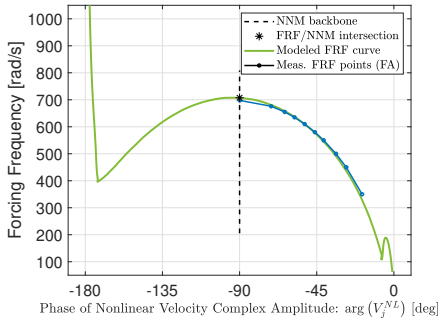

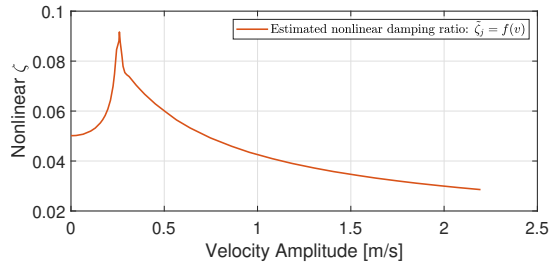

Validation

The upper (lag) and lower (lead) branches of the FRF are modeled using Eq. (4) with $(v_*,\ \omega_*)$ as a start point.

Modeled FRF is validated against the one measured using the numerical Force Appropriation method.

Tab. 29: Curved CC-Beam Numerical Example. Comparison of the nonlinear FRF curves modeled and measured numerically using Force Appropriation. FRF ID: 18

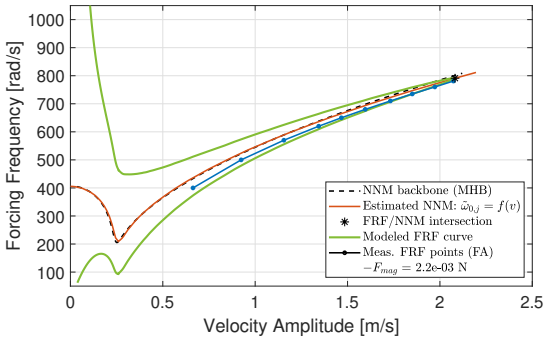

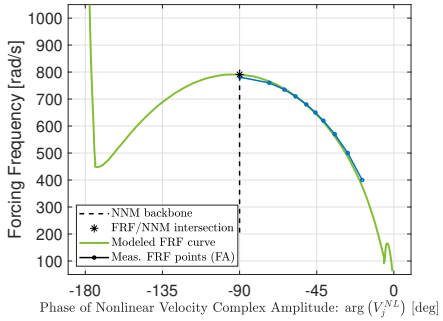

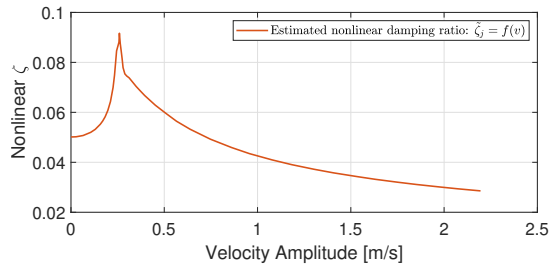

Validation

The upper (lag) and lower (lead) branches of the FRF are modeled using Eq. (4) with $(v_*,\ \omega_*)$ as a start point.

Modeled FRF is validated against the one measured using the numerical Force Appropriation method.

Comments

1. Proposed algorithm estimates the NNM backbone with a satisfactory precision using near-resonant test data (MIF $\in (0.7842,\ 1.0)$).

2. NNM points estimated using Eq. (4) for a given forcing magnitude are close enough to the resonant points measured numerically using Force Appropriation method and the same force amplitude .

3. Nonlinear frequency response functions measured numerically and computed using Eq. (4) match each other to a satisfactory extent.

4. The algorithm allows on significant reduction in the time spent on numerical measurements. Finding NNM curve using FA software takes approximately 2 hours 30 minutes. With the proposed algorithm, it takes approximately 1 hour.

5. Besides estimating the NNM backbone curve, the algorithm expresses nonlinear damping ratio as a function of velocity amplitude. In this particular example $\tilde{\zeta}_j$ is found as an increasing (decreasing) function when the system exhibits softening (stiffening).

3.3 3D Printing Process and Experimental Setup

Beam specimens employed in the experimental case study are 3D printed using polylactide (PLA). A brief description of the 3D printing process and the experimental setup is provided in this section.

3D Printing Process

As presented in Figs. 10 and 11a, the specimens are modeled using Solidworks [11]. They consist of thin and thick parts, called in this report beam (or thin beam) and backing (or thick beam), respectively. Former is the actual beam tested and latter is used to connect the structure to the shaker. Beam models are then exported to the UlitimateCura software [12] where the parameters concerning 3D printing process (e.g. layer height, walls thickness, nozzle size and speed, plate temperature, etc.) are specified, see Fig. 11c. One of the 3D printed beams is shown in Fig. 11b.

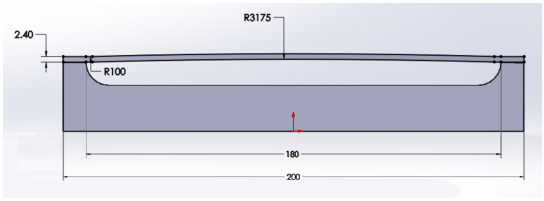

Fig. 10: Longitudinal cross-section of a 3D printed beam.

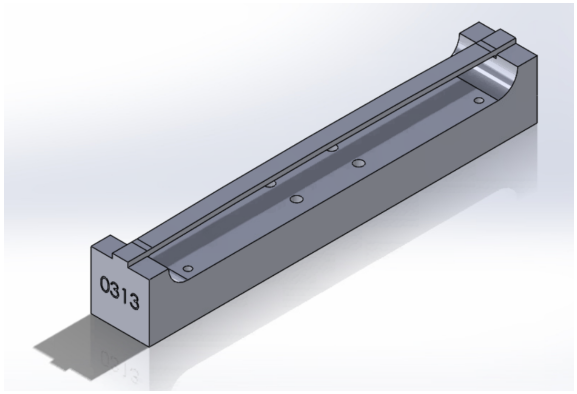

(a)

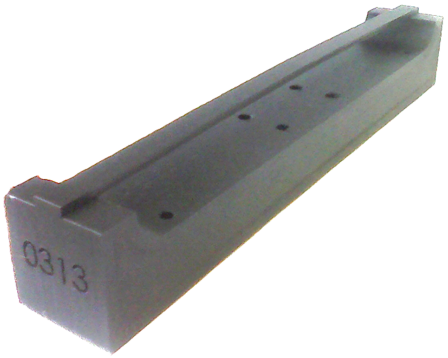

(b)

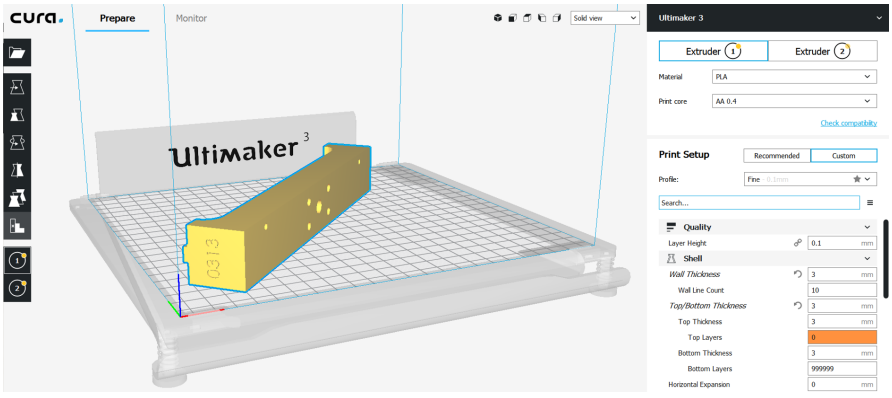

(c)

Fig. 11: 3D Printing Process: **(a)** SolidWorks model [11]; **(b)** Photograph of 3D Printed Beam; **(c)** Screen shot of 3D Printing Software Setup [12].

Experimental Setup

The experimental setup is shown in Fig. 12. It consists of three systems: (*i*) shaker, (*ii*) scanning laser vibrometer and (*iii*) force appropriation control system, which are described briefly below.

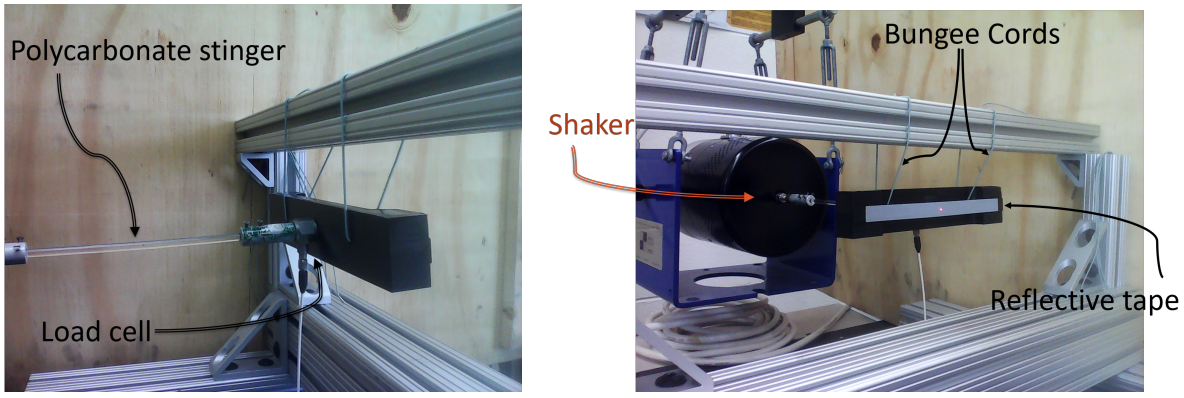

(a) **(b)**

Fig. 12: Photographs of experimental setup: **(a)** back view; **(b)** front view.

(*i*) The 3D printed beams are connected to the shaker using a polycarbonate stinger (as presented in Fig. 12). The input force applied to the backing of the specimens is measured with a load cell mounted at the singer's end. Unfortunately, the quality of the signal measured at the load cell is low, which is most likely caused by the oscillating structure feedback. Thus, signal sent from the controller was converted to the force units and used instead of the signal measured by the load cell

(*ii*) Polytec PSV–400M scanning laser vibrometer was used to capture the motion of the oscillating beam. The geometry of the beam was represented using a rectangular grid. Using the LabView control system, the thin beam is brought to the near-resonant state and then its full-field dynamic response is scanned over a several cycles using the Polytec software.

(*iii*) The force appropriation procedure was similar to the one described in [7]. The control system (created using LabView) allows on modifying the amplitude and frequency of the force with the voltage signal sent to the shaker. The phase between the voltage signal and the velocity of the beam's center (measured using the LDV) are is monitored (in real time) in order to indicate how far the structure is from oscillating at its nonlinear resonance (as explained in section 1.2).

3.4 3D Printed Curved Beam

The laboratory Force Appropriation test is performed on a *3D printed curved beam* (Beam ID: 0701a) made of polylactide (PLA). The beam has dimensions and mechanical parameters presented in Tab 30 and in Fig. 13. External force applied at the center of the backing is converted to uniformly distributed sinusoidal force $f(t)$ of magnitude F_{mag} (Fig. 14); $f(t)$ is then used in the system identification algorithm.

Tab. 30: Dimensions and mechanical properties of the 3D printed curved beam 0701a.

Lenght [mm]	Beam mass [g]	Backing mass [g]	Radius of curvature [mm]
190	3.7696	130	3175

Beam thickness [mm]	Beam width [mm]	Backing thickness [mm]
2.0	8.0	30.0

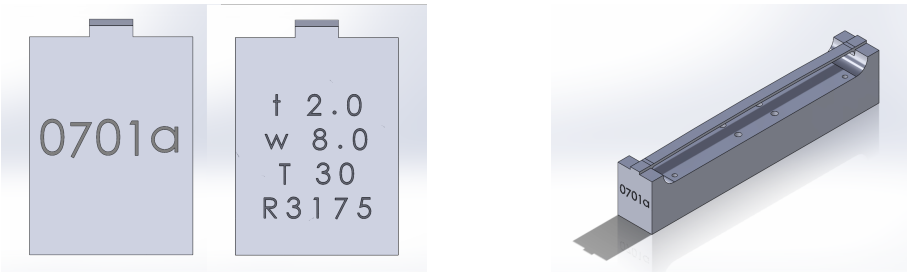

Fig. 13: (Left) Side views of 3D printed beam 0701a. Beam is signed and has its characteristic dimensions engraved on its sides. (Right) Isometric view of the beam.

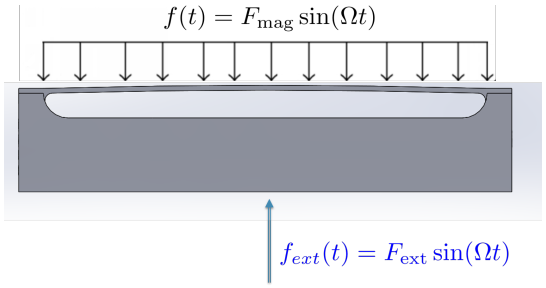

Fig. 14: Forcing was modeled as uniformly distributed sinusoidal excitation. It was converted from the external point-force applied at the center of beam 0701a backing.

Table 31 shows the results obtained after running the three-stages-long algorithm described in section 2.2. Plots corresponding to the validation part are presented in Tables from 32 to **??**. Results are briefly commented at the end of this section.

Tab. 31: 3D Printed Curved Beam Example. Results.

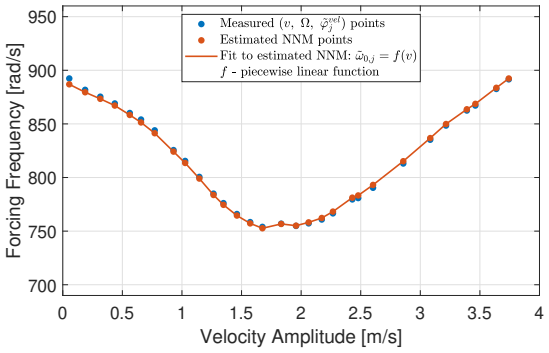

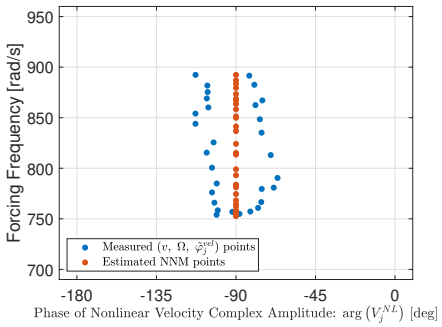

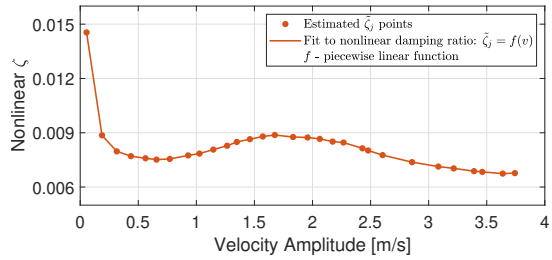

1) Near resonant data points have been collected; MIF $\in$ (0.8410, 0.9988).

2) The NNM points are estimated using Eqs. (4) and (9).

3) Piecewise linear function is used to approximate the NNM curve.

Tab. 32: 3D Printed Curved Beam Example. Comparison of the NNM points modeled and measured experimentally using Force Appropriation.

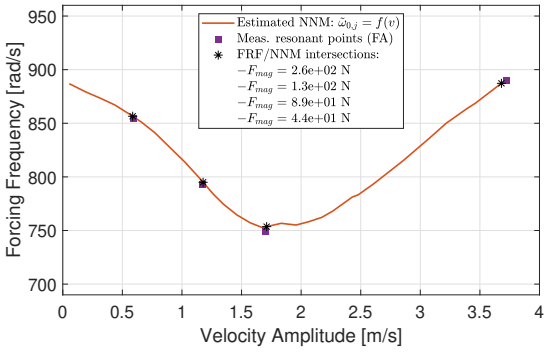

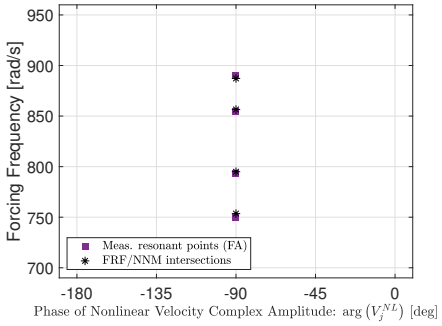

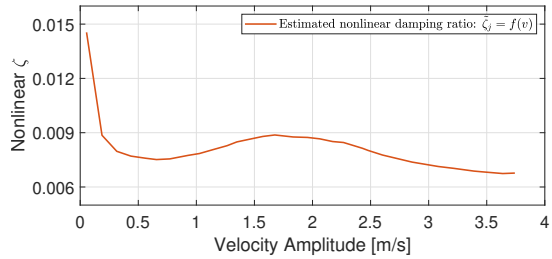

Validation

Points $(v_*,\ \omega_*)$ at which the FRF and NNM curves intersect for a certain forcing level are compared to the NNM points measured experimentally.

At the nonlinear resonance, forcing frequency and nonlinear modal frequency are equal: $\Omega = \tilde{\omega}_{0,j}(v_*) = \omega_*$. Hence, Eq. (4) at this point can be simplified:

$$v_* = \left\| \left(\frac{\boldsymbol{\Phi}_j \boldsymbol{\Phi}_j^T \mathbf{F}}{2i\tilde{\zeta}_j \omega_*} + \mathbf{V}^{lin}(\omega_*) \right) \Big|_{\substack{\text{pt. of max.} \\ \text{deflection}}} \right\|$$

Tab. 33: 3D Printed Curved Beam Example. Comparison of the nonlinear FRF curves modeled and measured experimentally using Force Appropriation. FRF ID: 1

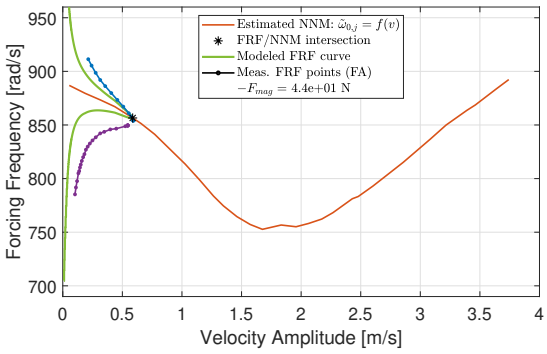

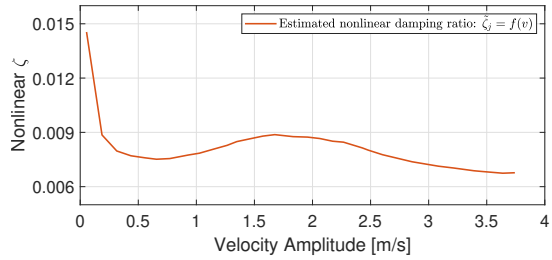

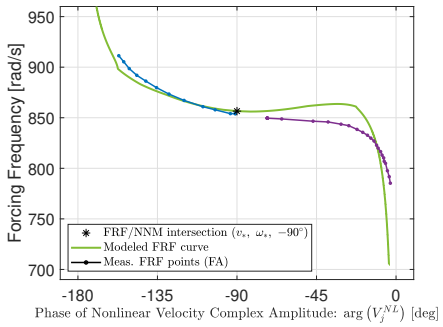

Validation

The upper (lag) and lower (lead) branches of the FRF are modeled using Eq. (4) with $(v_*,\ \omega_*)$ as a start point.

Modeled FRF is validated against the one measured using experimental Force Appropriation software.

Tab. 34: 3D Printed Curved Beam Example. Comparison of the nonlinear FRF curves modeled and measured experimentally using Force Appropriation. FRF ID: 2

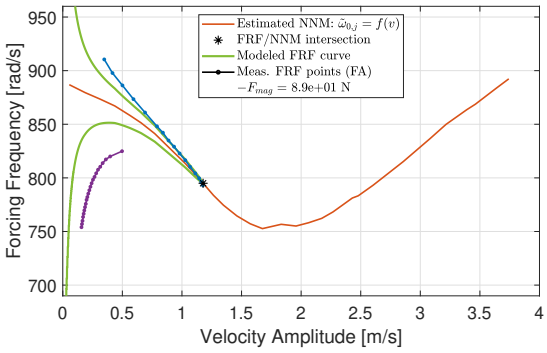

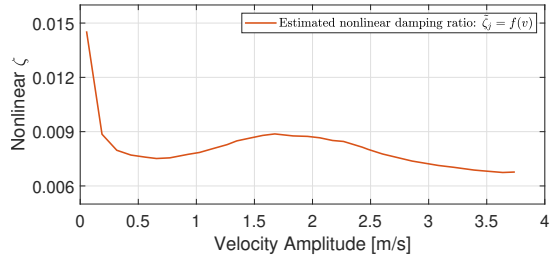

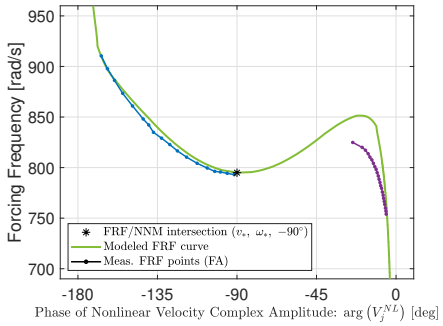

Validation

The upper (lag) and lower (lead) branches of the FRF are modeled using Eq. (4) with $(v_*,\ \omega_*)$ as a start point.

Modeled FRF is validated against the one measured using experimental Force Appropriation software.

Tab. 35: 3D Printed Curved Beam Example. Comparison of the nonlinear FRF curves modeled and measured experimentally using Force Appropriation. FRF ID: 3

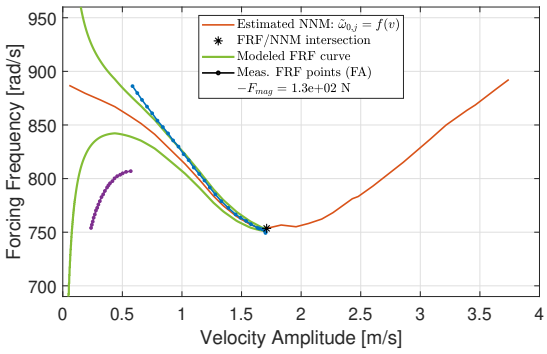

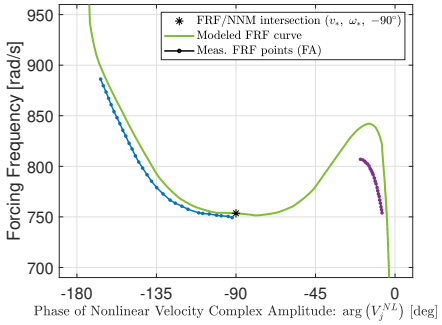

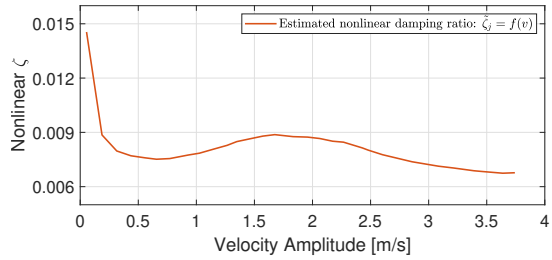

Validation

The upper (lag) and lower (lead) branches of the FRF are modeled using Eq. (4) with $(v_*,\ \omega_*)$ as a start point.

Modeled FRF is validated against the one measured using experimental Force Appropriation software.

Tab. 36: 3D Printed Curved Beam Example. Comparison of the nonlinear FRF curves modeled and measured experimentally using Force Appropriation. FRF ID: 4

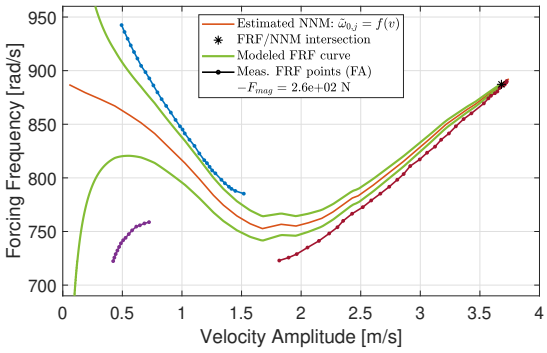

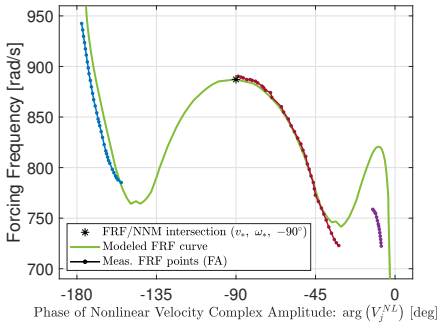

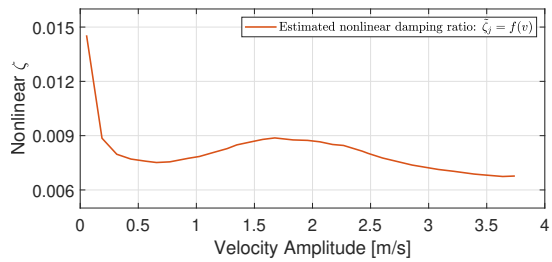

Validation

The upper (lag) and lower (lead) branches of the FRF are modeled using Eq. (4) with $(v_*,\ \omega_*)$ as a start point.

Modeled FRF is validated against the one measured using experimental Force Appropriation software.

Comments

1. Proposed algorithm estimates the NNM backbone with a satisfactory precision using near-resonant test data (MIF $\in (0.8410,\ 0.9988)$).

2. NNM points estimated using Eq. (4) for a given forcing magnitude are close enough to the resonant points measured numerically using Force Appropriation method and the same force amplitude .

3. Nonlinear frequency response functions measured numerically and computed using Eq. (4) match each other to a satisfactory extent. The proposed algorithm is currently based on a model which does not include Rigid Body Modes in its modal basis. This is (most likely) the cause of the discrepancy between the FRF branches modeled and measured at low frequencies.

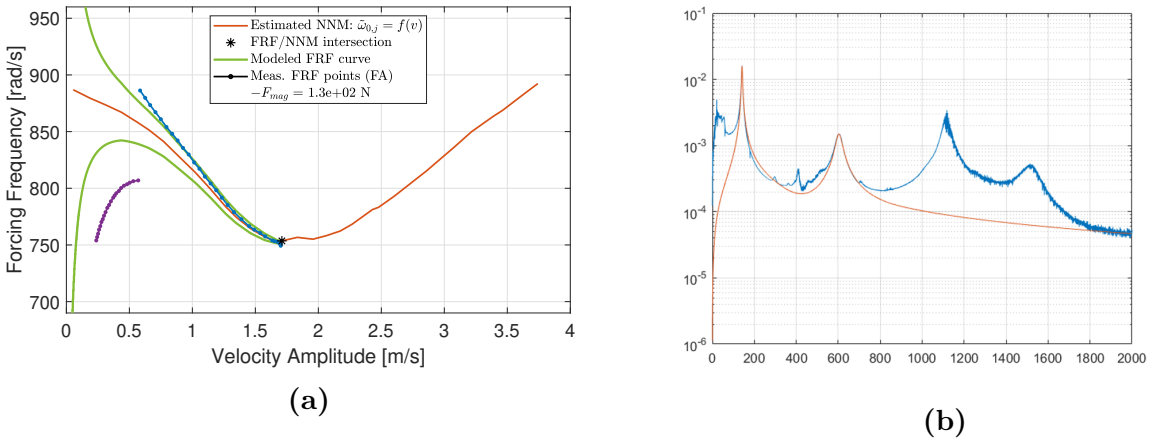

(a) **(b)**

Fig. 15: The proposed algorithm is currently based on a model which does not include Rigid Body Modes in its modal basis. This is (most likely) the cause of the discrepancy between the FRF branches modeled and measured at low frequencies. **(a)** Comparison of the measured and modeled FRFs; **(b)** Fit to the measured FRF - obtained using AMI software [13–15].

4. The algorithm allows on significant reduction in the time spent on numerical measurements. Finding NNM curve experimentally using FA software takes approximately 4 hours. With the proposed algorithm, it takes approximately 1 hour.

5. Besides estimating the NNM backbone curve, the algorithm expresses nonlinear damping ratio as a function of velocity amplitude. In this particular example $\tilde{\zeta}_j$ is found as an increasing (decreasing) function when the system exhibits softening (stiffening).

3.5 3D Printed Flat Beam

The laboratory Force Appropriation test is performed on a *3D printed flat beam* (Beam ID: 0701c) made of polylactide (PLA). The beam has dimensions and mechanical parameters presented in Tab 37 and in Fig. 16. External force applied at the center of the backing is converted to uniformly distributed sinusoidal force $f(t)$ of magnitude F_{mag} (Fig. 17); $f(t)$ is then used in the system identification algorithm.

Tab. 37: Dimensions and mechanical properties of the 3D printed flat beam.

Lenght [mm]	Beam mass [g]	Backing mass [g]	Radius of curvature
190	3.7696	130	∞
Beam thickness [mm]	**Beam width [mm]**	**Backing thickness [mm]**	
2.0	8.0	30.0	

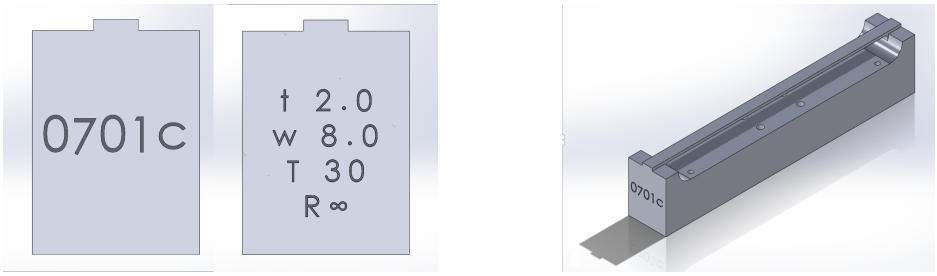

Fig. 16: (Left) Side views of 3D printed beam 0701c. Beam is signed and has its characteristic dimensions engraved on its sides. (Right) Isometric view of the beam

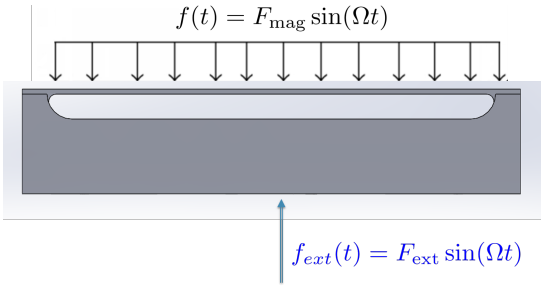

Fig. 17: Forcing was modeled as uniformly distributed sinusoidal excitation. It was converted from the external point-force applied at the center of beam 0701c backing.

Table 38 shows the results obtained after running three-stages-long algorithm described in section 2.2. Plots corresponding to the validation part are presented in Tables from 39 to 41. Results are briefly commented at the end of this section.

Tab. 38: 3D Printed Flat Beam Example. Results.

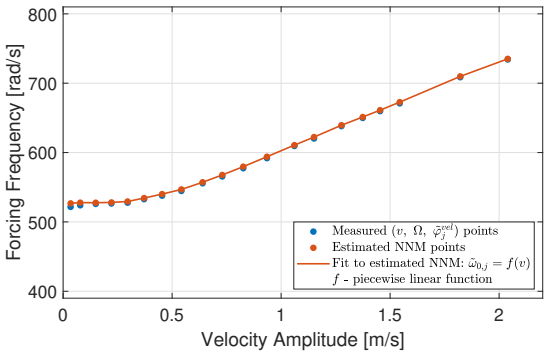

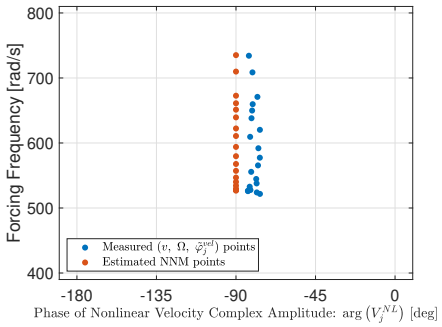

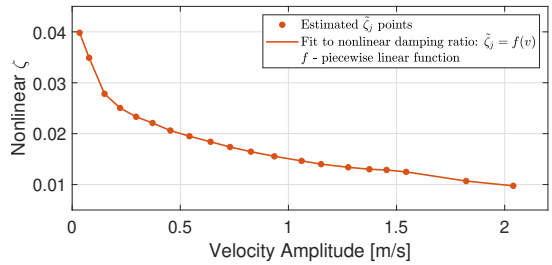

1) Near resonant data points have been collected; MIF $\in (0.845,\ 0.986)$.

2) The NNM points are estimated using Eqs. (4) and (9).

3) Piecewise linear function is used to approximate the NNM curve.

Tab. 39: 3D Printed Flat Beam Example. Comparison of the NNM points modeled and measured experimentally using Force Appropriation.

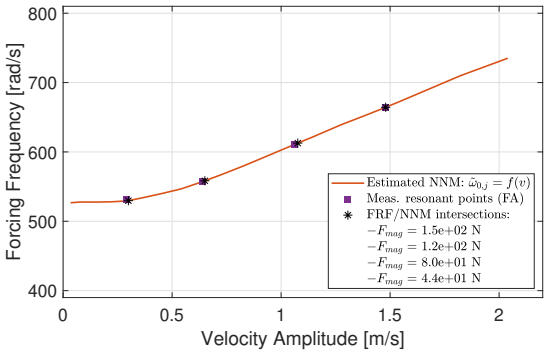

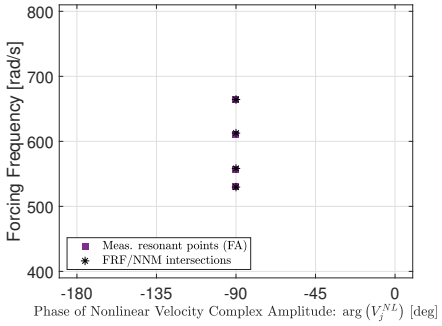

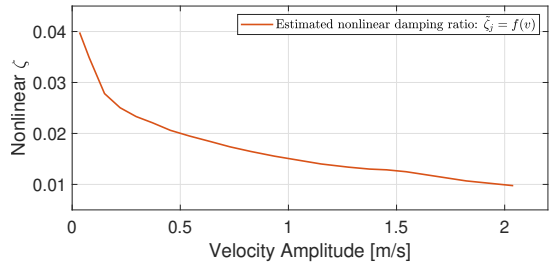

Validation

Points $(v_*,\ \omega_*)$ at which the FRF and NNM curves intersect for a certain forcing level are compared to the NNM points measured experimentally.

At the nonlinear resonance, forcing frequency and nonlinear modal frequency are equal: $\Omega = \tilde{\omega}_{0,j}(v_*) = \omega_*$. Hence, Eq. (4) at this point can be simplified:

$$v_* = \left\| \left(\frac{\boldsymbol{\Phi}_j \boldsymbol{\Phi}_j^T \mathbf{F}}{2i\tilde{\zeta}_j \omega_*} + \mathbf{V}^{lin}(\omega_*) \right) \Big|_{\substack{\text{pt. of max.} \\ \text{deflection}}} \right\|$$

Tab. 40: 3D Printed Flat Beam Example. The nonlinear FRF curve modeled using Eq. (4).

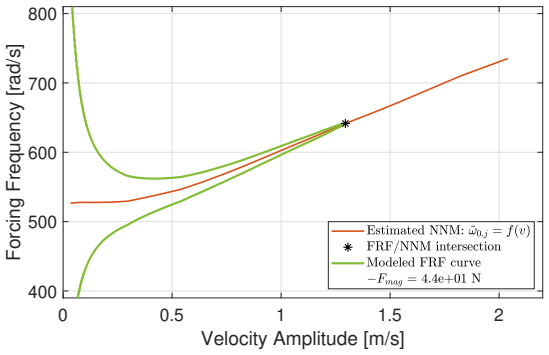

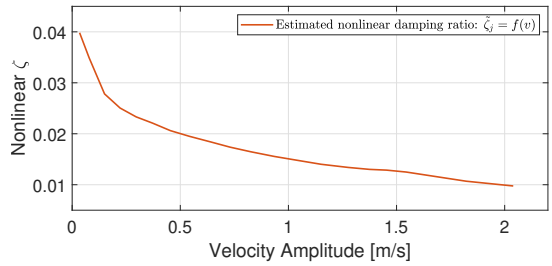

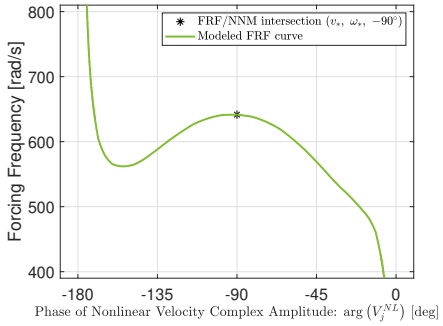

Validation

The upper (lag) and lower (lead) branches of the FRF are modeled using Eq. (4) with $(v_*,\ \omega_*)$ as a start point.

Curve presented in the chart is the FRF computed for the uniformly distributed forcing with $F_{mag} \approx 44$ N.

Tab. 41: 3D Printed Flat Beam Example. Comparison of the nonlinear FRF curves modeled and measured experimentally using Force Appropriation.

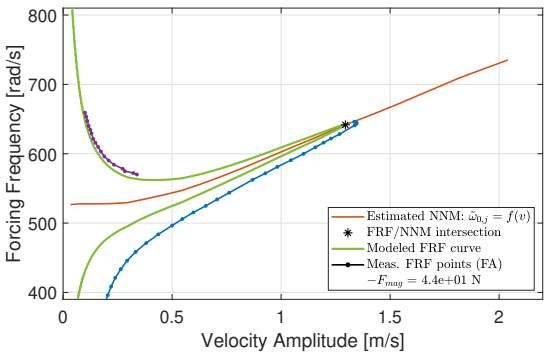

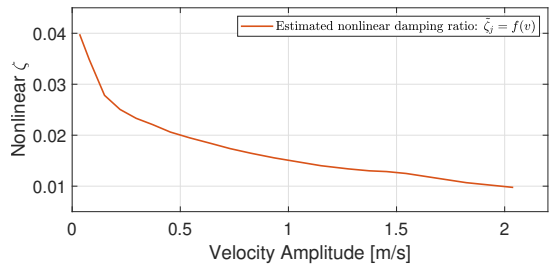

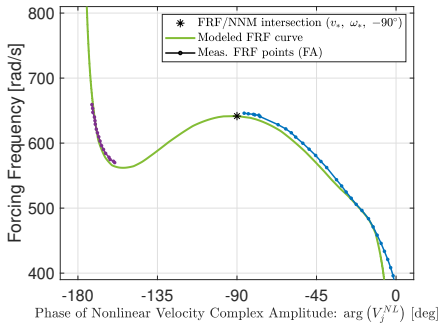

Validation

The upper (lag) and lower (lead) branches of the FRF are modeled using Eq. (4) with $(v_*,\ \omega_*)$ as a start point.

Curves presented in the chart are the FRFs computed for the uniformly distributed forcing with $F_{mag} \approx 44$ N.

Results are compared to the FRF measured experimentally using Force Appropriation.

Comments

1. Proposed algorithm estimates the NNM backbone with a satisfactory precision using near-resonant test data (MIF $\in (0.945,\ 0.986)$).

2. NNM points estimated using Eq. (4) for a given forcing magnitude are close enough to the resonant points measured numerically using Force Appropriation method and the same force amplitude .

3. Nonlinear frequency response functions measured numerically and computed using Eq. (4) match each other to a satisfactory extent. The proposed algorithm is currently based on a model which does not include Rigid Body Modes in its modal basis. This is (most likely) the cause of the discrepancy between the FRF branches modeled and measured at low frequencies.

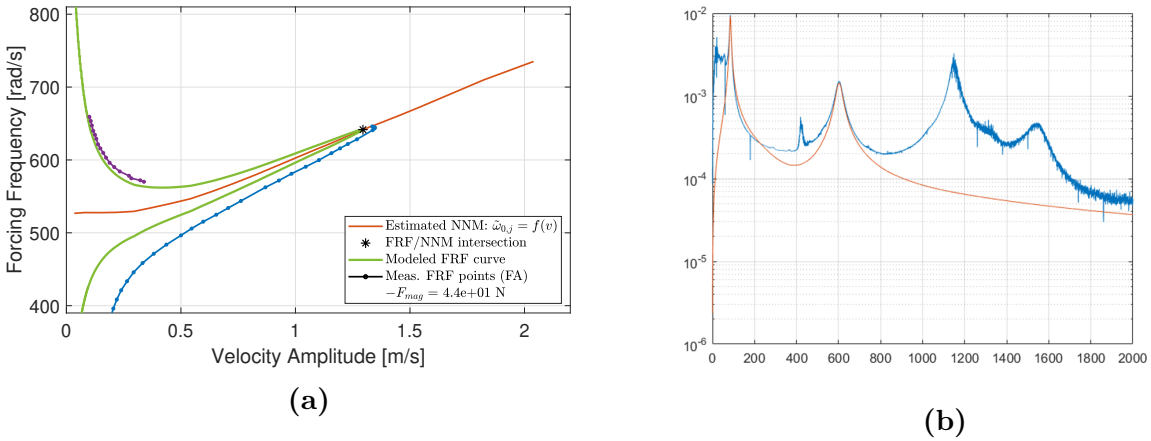

(a) **(b)**

Fig. 18: The proposed algorithm is currently based on a model which does not include Rigid Body Modes in its modal basis. This is (most likely) the cause of the discrepancy between the FRF branches modeled and measured at low frequencies. **(a)** Comparison of the measured and modeled FRFs; **(b)** Fit to the measured FRF - obtained using AMI software [13–15].

4. The algorithm allows on significant reduction in the time spent on numerical measurements. Finding NNM curve using FA software takes approximately 2 hours 30 minutes. With the proposed algorithm, it takes approximately 1 hour.

5. Besides estimating the NNM backbone curve, the algorithm expresses nonlinear damping ratio as a function of velocity amplitude. In this particular example $\tilde{\zeta}_j$ is found as a decreasing function of the vibration level.

4 Summary and Future Work

Summary

1. Proposed algorithm estimates the NNM backbone with a satisfactory precision using near-resonant test data.
2. The algorithm allows on significant reduction in the time spent on experimental/numerical measurements.
3. The software requires Minimal User Interaction. After collecting the data – the NNM estimation process takes approx. 1 minute and needs only a couple of mouse/button clicks.

Future Steps

1. Adding the Rigid Body Mode to the Frequency Response model.
2. Modifying the algorithm such that it:
   - allows multi-harmonic input
   - can be used in analyzing systems experiencing modal coupling.
3. Using the algorithm to predict the nonlinear vibration of structure different than 3D printed beam, e.g. steel beam, perforated plate, gong, crystal glass, etc.

References

[1] Kerschen, G., Peeters, M., Golinval, J., and Vakakis, A., 2009. "Nonlinear normal modes, Part I: A useful framework for the structural dynamicist". *Mechanical Systems and Signal Processing,* **23**(1), pp. 170 – 194. Special Issue: Non-linear Structural Dynamics.

[2] Peeters, M., Viguié, R., Sérandour, G., Kerschen, G., and Golinval, J.-C., 2009. "Nonlinear normal modes, Part II: Toward a practical computation using numerical continuation techniques". *Mechanical Systems and Signal Processing,* **23**, 01, pp. 195–216.

[3] Krack, M., 2015. "Nonlinear modal analysis of nonconservative systems: Extension of the periodic motion concept". *Computers & Structures,* **154**, 07.

[4] Rosenberg, R. M., 1960. "Normal Modes of Nonlinear Dual-Mode Systems". *Journal of Applied Mechanics,* **27**, pp. 263 – 268.

[5] Vakakis, A., 1997. "Non-linear normal modes (nnms) and their applications in vibration theory: An overview". *Mechanical Systems and Signal Processing,* **11**(1), pp. 3 – 22.

[6] Ehrhardt, D. A., Allen, M. S., and Beberniss, T. J., 2016. "Measurement of Nonlinear Normal Modes Using Mono-harmonic Force Appropriation: Experimental Investigation". In Nonlinear Dynamics, Volume 1, G. Kerschen, ed., Springer International Publishing, pp. 241–254.

[7] Ehrhardt, D. A., and Allen, M. S., 2016. "Measurement of nonlinear normal modes using multi-harmonic stepped force appropriation and free decay". *Mechanical Systems and Signal Processing,* **76-77**, pp. 612 – 633.

[8] Szemplińska-Stupnicka, W., 1979. "The modified single mode method in the investigations of the resonant vibrations of non-linear systems". *Journal of Sound and Vibration,* **63**(4), pp. 475 – 489.

[9] Peter, S., Scheel, M., Krack, M., and Leine, R. I., 2018. "Synthesis of nonlinear frequency responses with experimentally extracted nonlinear modes". *Mechanical Systems and Signal Processing,* **101**, pp. 498 – 515.

[10] Hollkamp, J. J., Gordon, R. W., and Spottswood, S. M., 2005. "Nonlinear modal models for sonic fatigue response prediction: a comparison of methods". *Journal of Sound and Vibration,* **284**(3), pp. 1145 – 1163.

[11] Dassault Systèmes, 2018. SolidWorks. `https://www.solidworks.com`. Version 2018. Accessed: August 09 2019.

[12] Ultimaker, 2017. Ultimaker Cura: 3D Printing Software. `https://ultimaker.com/software/ultimaker-cura`. Version 3.0. Accessed: August 05 2019.

[13] Ginsberg, J. H., and Allen, M. S., 2004. "A linear least-squares version of the algorithm of mode isolation for identifying modal properties. Part I: Conceptual development". *The Journal of the Acoustical Society of America,* **116**(2).

[14] Allen, M. S., and Ginsberg, J. H., 2004. "A linear least-squares version of the algorithm of mode isolation for identifying modal properties. Part II: Application and assessment". *The Journal of the Acoustical Society of America,* **116**(2).

[15] Allen, M. S., and Ginsberg, J. H., 2006. "A global, single-input–multi-output (simo) implementation of the algorithm of mode isolation and application to analytical and experimental data". *Mechanical Systems and Signal Processing,* **20**(5).